NATIONAL ADVISORY COMMITTEE FOR AERONAUTICS

WARTIME REPORT

ORIGINALLY ISSUED

July 1944 as
Advance Restricted Report E4G20

COMPRESSIBILITY AND HEATING EFFECTS ON PRESSURE LOSS AND COOLING OF A BAFFLED CYLINDER BARREL

By Arthur W. Goldstein and Herman H. Ellerbrock, Jr.

Aircraft Engine Research Laboratory
Cleveland, Ohio

NACA

WASHINGTON

NACA ARR No. E4G20

NATIONAL ADVISORY COMMITTEE FOR AERONAUTICS

ADVANCE RESTRICTED REPORT

COMPRESSIBILITY AND HEATING EFFECTS ON PRESSURE LOSS AND COOLING OF A BAFFLED CYLINDER BARREL

By Arthur W. Goldstein and Herman H. Ellerbrock, Jr.

SUMMARY

Theoretical investigations have shown that, because air is compressible, the pressure-drop requirements for cooling an air-cooled engine will be much greater at high altitudes and high speeds than at sea level and low speeds. Tests were conducted by the NACA to obtain some experimental confirmation of the effect of air compressibility on cooling and pressure loss of a baffled cylinder barrel and to evaluate various methods of analysis. The results reported in the present paper are regarded as preliminary to tests on single-cylinder and multicylinder engines. Tests were conducted over a wide range of air flows and density altitudes.

The results indicate that, for a given air weight flow, the reduced pressure drop based on average cooling-air density $\Delta p \rho_{av}/\rho_s$, which has been used to correlate heat-transfer cooling data, is not constant for different air densities (Δp, cooling-air pressure drop across the engine; ρ_{av}/ρ_s, ratio of average cooling-air density to density at sea level). Engine-cooling variables should therefore not be plotted against pressure drop. From the present tests a correlating variable for heat-transfer data is shown to be the air weight flow; the reduced pressure drop is not suitable for this purpose. An analysis based on the assumption of uniform flow is shown to be satisfactory for estimating the effect of compressibility on data obtained in these tests. A simpler empirical method in which compressibility and heating effects can be estimated was found for correlating the test data on pressure loss.

INTRODUCTION

Some investigators have heretofore correlated cooling data for air-cooled engines with the cooling-air pressure drop (references 1 to 4). The effect of compressibility was taken into account by using the product of the pressure drop and the average of the air densities

at the front and the rear of the cylinder as the correlating variable rather than the pressure drop alone. With the high rate of heat exchange and the high air velocity between the fins required for effective cooling at high altitudes, however, a large air-density change will result. This change in air density is attended by an increase in velocity, and an additional pressure loss will be incurred at the baffle exit where this momentum will be lost. Estimates of the increase in pressure loss caused by air compressibility in engine-cooling systems with baffled cylinders were made in references 5 to 9. The analyses of references 5 and 9 were based on the assumptions of one-dimensional gas dynamics, but no experimental data were available to support these analyses.

An investigation was begun by the NACA to obtain experimental confirmation of the effect of compressibility and rate of heat transfer on pressure loss and cooling of a baffled section of a cylinder barrel and to evaluate the various methods of correlating these data. The tests covered a range of simulated density altitudes from 4000 to 33,000 feet, of velocities between the fins from a Mach number of 0.05 to near sonic values, and of heat inputs from 0 to 500 Btu per hour per square inch of cylinder-wall surface. This investigation was conducted at Langley Memorial Aeronautical Laboratory, Langley Field, Va., during 1942.

Acknowledgment is made to Mr. Frank E. Marble of the Supercharger and Airflow Research Division, Aircraft Engine Research Laboratory of the NACA for his suggestion that the Prandtl-Glauert compressibility factor be used to correlate the results of the present tests.

ANALYSIS

One-Dimensional Gas Dynamics

The analysis of the flow around a baffled cylinder is based on the assumptions of one-dimensional gas dynamics. The equations for the pressure and density changes through a baffled-cylinder system (fig. 1) are developed by the following analysis, which is similar to that of reference 5.

1. The heat transfer between stations 1 and 2 and between stations 2 and 4 is estimated.

2. No loss in total pressure is assumed from station 1 to station 2.

3. The pressure and the density at station 2 are then calculated from the heat-transfer estimate, the stagnation pressure, and the mass flow.

4. The analysis of the flow between stations 2 and 3 is based on the assumption of uniform flow of a compressible fluid with friction in a straight duct.

5. The loss at the baffle exit is computed from the momentum equations for uniform flow at stations 3 and 4.

Change in gas state between station 1 and station 2. - If the heat picked up by the air between station 1 and station 2 and the weight of air flowing through the baffle are known,

$$H_1 = Wc_p\left(T_{2_t} - T_{1_t}\right) \tag{1}$$

where

H_1 rate of heat transfer to air between stations 1 and 2, Btu per second (The method of obtaining H_1 is given in appendix A.)

W weight of air flowing through baffle, pounds per second

c_p specific heat of air at constant pressure, Btu per pound per $^{\circ}F$

T_{2_t} stagnation temperature at station 2, $^{\circ}F$ absolute

T_{1_t} stagnation temperature at station 1, $^{\circ}F$ absolute

A complete list of the symbols used is presented in appendix B.

Stagnation or total temperature and pressure as used in this report indicate gas properties that would obtain if the kinetic energy of the moving gas were isentropically converted into enthalpy. The temperature T_{1_t} may be considered equal to the static temperature at station 1 because the velocity at station 1 is negligible. If T_{1_t}, W, and H_1 are known, the total temperature at station 2 may be obtained from equation (1).

The assumption is made that there is no loss in total pressure from station 1 to station 2 and that the stagnation state of the air at station 2 is known. Then, from the relations

$$\frac{W}{gA_2} = \rho_2 V_2 \tag{2}$$

and

$$M_2^2 = \frac{\rho_2 V_2^2}{\gamma p_2} \tag{3}$$

and by means of the relations for isentropic change, the true-stream density and pressure may be eliminated and the stagnation density and pressure inserted to give

$$\frac{(\rho_2 V_2)^2}{p_{2_t}\,\rho_{2_t}} = \frac{\gamma M_2^2}{\left[1 + \frac{\gamma - 1}{2} M_2^2\right]^{\frac{\gamma+1}{\gamma-1}}} \qquad (4)$$

where

g acceleration of gravity, feet per second^2

A_2 cross-sectional area of free-flow space at station 2, square feet

ρ_2 density of air at station 2, slugs per cubic foot (based on p_2 and T_2)

V_2 velocity of air in fin passage at station 2, feet per second

M_2 Mach number at station 2

γ ratio of specific heats for air (1.3947)

p_2 static pressure of air at station 2, pounds per square foot

p_{2_t} stagnation air pressure at station 2, pounds per square foot

ρ_{2_t} stagnation air density at station 2 (computed from p_{2_t} and T_{2_t}), slugs per cubic foot

T_2 true air-stream temperature of cooling air at station 2, $^\circ$F absolute

When $(\rho_2 V_2)^2 / p_{2_t} \rho_{2_t}$ is known, M_2 can be determined from equation (4); the ratios ρ_2/ρ_{2_t} and p_2/p_{2_t} can be determined from the isentropic-change relations. A chart based on equation (4) and the isentropic relations is given in figure 2.

Change in gas state between station 2 and station 3. - The pressure drop through the baffle from station 2 to station 3 is given by the following equation, which has been modified from the corresponding equation in reference 5 by inserting the value of C_{D_f} in terms of $C_{D_{f_i}}$,

$$\frac{p_2 - p_3}{q_2} = \frac{C_{D_{f_i}}}{2}\left(1 + \frac{\rho_2}{\rho_3}\right) + 2\left(\frac{\rho_2}{\rho_3} - 1\right) \tag{5}$$

where

q_2 dynamic pressure at station 2, $\left(\frac{1}{2}\rho_2 V_2^2\right)$, pounds per square foot

C_{D_f} friction-drag coefficient between stations 2 and 3 based on q_2, $\left(C_{D_f} \equiv \frac{D_f}{A_2 q_2}\right)$

$C_{D_{f_i}}$ friction-drag coefficient between station 2 and station 3 based on average of q_2 and q_3, $\left[C_{D_{f_i}} \equiv (D_f/A_2)\left(\frac{2}{q_2 + q_3}\right)\right]$

D_f friction drag from station 2 to station 3, pounds

q_3 dynamic pressure at station 3, $\left(\frac{1}{2}\rho_3 V_3^2\right)$, pounds per square foot

p_3 static pressure at station 3, pounds per square foot

ρ_3 density of air at station 3, slugs per cubic foot

V_3 velocity of air at station 3, feet per second

If the value for the local friction-drag coefficient $C_{D_{f_i}}$ is assumed constant for all elements of the path, D_f would actually be obtained by a process of integration. The value of $C_{D_{f_i}}$ should therefore be calculated from D_f by means of some integrated mean value for $\frac{1}{2}\rho V^2$. The value calculated from the arithmetical average of q_2 and q_3, however, is used as an approximation. If this approximation is good, $C_{D_{f_i}}$ thus calculated should be independent of inlet-density variations for fixed values of Reynolds number and equal to the value that would be obtained with an incompressible fluid. By means of the continuity equation, the relationship between C_{D_f} and $C_{D_{f_i}}$ can be established as

$$C_{D_f} = \frac{C_{D_{f_i}}}{2}\left(1 + \frac{\rho_2}{\rho_3}\right) \tag{6}$$

The density ratio required for the solution of equation (5) can be calculated from the following equation, which is modified from the corresponding equation in reference 5 by inserting the value for C_{D_f} in terms of $C_{D_{f_i}}$ to give

$$\frac{\rho_2}{\rho_3} = 1 + \frac{H_2}{c_p W T_2} + \frac{\gamma-1}{2} M_2^2 \left\{ 1 - \left(\frac{\rho_2}{\rho_3}\right)^2 + \frac{2\gamma}{\gamma-1}\left(\frac{\rho_2}{\rho_3}\right)\left[\frac{C_{D_{f_i}}}{4}\left(1+\frac{\rho_2}{\rho_3}\right) + \frac{\rho_2}{\rho_3} - 1\right]\right\} \tag{7}$$

where

H_2 rate of heat transfer to air between stations 2 and 3, Btu per second (The method of determining H_2 is given in appendix A.)

A convenient method of determining ρ_2/ρ_3 uses the variables

$$T' \equiv \frac{H_2}{c_p W T_2} \tag{8}$$

$$\rho' \equiv \rho_2/\rho_3 \tag{9}$$

$$M_a^2 \equiv \frac{\rho' - 1}{\gamma\rho'\left[\frac{C_{D_{f_i}}}{4}(1+\rho') + (\rho'-1)\right] + \frac{\gamma-1}{2}\left(1-\rho'^2\right)} \tag{10}$$

$$M_b^2 \equiv \frac{M_a^2}{\rho' - 1} \tag{11}$$

When use is made of these definitions, equation (7) becomes

$$M_a^2 = M_2^2 + T' M_b^2 \tag{12}$$

Because M_a^2 and M_b^2 are functions only of ρ' and $C_{D_{f_i}}$, for each value of $C_{D_{f_i}}$ the variable M_a^2 may be plotted against M_b^2 and ρ' may be plotted against M_a^2 by use of the definitions for M_a^2 and M_b^2. These plots are shown in figure 3. The value M_a^2 must, however, be the ordinate satisfying the linear equation (12) with M_2^2 as the y intercept, M_b^2 as the abscissa, and T' as the slope. The intersection of this line with the curve of M_a^2

against M_b^2 for the given $C_{D_{f_i}}$ determines M_a^2. From the curve of M_a^2 against ρ' for the given $C_{D_{f_i}}$ the value of ρ' can be obtained.

Change in gas state between station 3 and station 4. - The momentum equation characterizing the pressure loss between station 3 and station 4 is derived for the baffle with a tailpiece. This loss as given in references 5 and 9 was for a baffle without a tailpiece, where station 4 was in a section of very large area with very low velocity. For the present case the momentum equation is

$$p_3 A_3 \sin \theta_3 - p_4 A_4 + \int p dS_x - D_3 = \frac{W}{g} (V_4 - V_3 \sin \theta_3) \qquad (13)$$

where

θ_3 angle between radii of cylinder to cylinder rear and to station 3, degrees (See fig. 1.)

p_4 static pressure at station 4, pounds per square foot

A_3 cross-sectional area at station 3, square feet

A_4 cross-sectional area of baffle exit at station 4, square feet

p static pressure, pounds per square foot

dS_x projection of any element of cylinder-wall surface and of curved part of baffle surface back of station 3 on plane of A_4, square feet

D_3 component of drag force normal to plane of A_4 and effective between stations 3 and 4, pounds

V_4 velocity of air at station 4, feet per second

The integral of pdS_x is taken over the entire surface bounding the fluid between stations 3 and 4 except at flow cross sections of stations 3 and 4.

It can be shown that

$$\int dS_x = A_4 - A_3 \sin \theta_3 \qquad (14)$$

The pressure gradients will be proportional to the kinetic energy at station 3. Therefore, if

$$a_3 \equiv \int \frac{(p - p_3)\, dS_x}{\frac{1}{2} \rho_3 V_3^2 A_4} \tag{15}$$

if the coefficient for friction drag in the baffle exit is

$$C_3 \equiv \frac{D_3}{\frac{1}{2} \rho_3 V_3^2 A_4} \tag{16}$$

and, if these symbols and the continuity equation are employed, the momentum equation may be expressed as

$$\frac{p_3 - p_4}{q_3} = C_3 - a_3 - 2 \frac{A_3}{A_4} \sin \theta_3 + 2\left(\frac{A_3}{A_4}\right)^2 \frac{\rho_3}{\rho_4} \tag{17}$$

In this equation the term $2(A_3/A_4) \sin \theta_3$ indicates that the momentum loss caused by the fact that the stream at the rear of the cylinder is not directed straight back cannot be neglected. This direction of the stream, however, tends to increase the value of a_3 and the pressure recovery. The recovery coefficient a_3, therefore, in some measure compensates for the fact that $\theta_3 \neq 90^\circ$. In the case of $A_3 << A_4$, all the terms become small and consequently p_3 is approximately equal to p_4.

For the present report the losses across the cylinder will be represented by equations (5) and (17). In the actual practice of predicting the pressure losses, once the coefficients of equation (17) are evaluated, the density change may be evaluated from equation (17) and the energy equation.

Application of Prandtl-Glauert Compressibility Factor to Flow across a Baffled Cylinder

The foregoing theory for flow of a compressible fluid is applicable only to the case of uniform velocity or one-dimensional flow. For two-dimensional flow, the Prandtl-Glauert factor $\sqrt{1 - M_o^2}$ is used to compute the effect of compressibility. The Prandtl-Glauert factor is strictly applicable in flow conditions quite different from those existing around the baffled cylinder now being considered; therefore, this name should not be used for this application of the factor but will be used for convenience. The proper application of this

factor is to static-pressure variations in the flow field of a body causing small perturbation velocities in an infinite uniform flow field with a frictionless, compressible fluid and with no heat transfer. In that case the difference in static pressure at any point in the flow field from what the static pressure would be with an incompressible fluid can be computed by the Prandtl-Glauert factor $\sqrt{1 - M_o^2}$ in the equation (reference 10)

$$C_{p_M} \equiv \frac{p - p_o}{q_o} = \frac{p_i - p_o}{q_o} \frac{1}{\sqrt{1 - M_o^2}} \tag{18}$$

or

$$C_{p_M} = \frac{C_{p_i}}{\sqrt{1 - M_o^2}} \tag{19}$$

where

p_o pressure of fluid that is characteristic of flow, pounds per square foot

q_o dynamic pressure of fluid that is characteristic of flow $\left(\frac{1}{2} \rho_o V_o^2\right)$, pounds per square foot

M_o Mach number that is characteristic of flow

p_i static pressure at same point as p with incompressible fluid, pounds per square foot

ρ_o density of fluid that is characteristic of flow, slugs per cubic foot

V_o velocity of fluid that is characteristic of flow, feet per second

C_{p_M} pressure-loss coefficient with compressible flow

C_{p_i} pressure-loss coefficient with incompressible flow

The factor $\sqrt{1 - M_o^2}$ was used to reduce the total-pressure-loss data to values that might be expected without compressibility effects. The application of the factor to the present data is to be regarded solely as an empirical method of correlation. No rational basis for the use of this factor is presented herein.

The pressure drop used in place of $p - p_o$ in equation (18) for the baffled cylinder is $p_{1_t} - p_{4_t}$. The method of calculating q_o and M_o was empirically determined by finding the pressure and the temperature that would give the best correlation of the data with different densities and various rates of heat transfer. The factor C_{p_i} was then computed

$$C_{p_i} = \frac{p_{1_t} - p_{4_t}}{q_o} \sqrt{1 - M_o^2} \tag{20}$$

The total-pressure loss to be expected with an incompressible fluid Δp_i is then

$$\Delta p_i = C_{p_i} q_o = C_{p_i} \frac{(\rho V)^2}{2\rho_o} \tag{21}$$

For the same mass flow (ρV) but with standard density ρ_s, C_{p_i} will remain constant because it depends on only the Reynolds number. Then

$$\Delta p_{i_s} = \Delta p_i \rho_o / \rho_s \tag{22}$$

where

Δp_{i_s} loss in total pressure under standard density conditions, pounds per square foot

ρ_s standard density (at 29.92 in. Hg and 60° F), slugs per cubic foot

From equations (20), (21), and (22)

$$\Delta p_{i_s} = \Delta p_t \frac{\rho_o}{\rho_s} \sqrt{1 - M_o^2} \tag{23}$$

where

$$\Delta p_t \equiv p_{1_t} - p_{4_t}$$

The Effect of Compressibility on Heat Transfer

The effect of compressibility on the heat-transfer coefficients is estimated by the effect calculated for a flat plate by an equation given in reference 11. If the temperature of the plate is assumed to

be 300° F (an average fin and cylinder temperature to be expected with a 450° F rear spark-plug temperature), the Reynolds number is assumed to be 3000, and the free-stream air temperature is assumed to be -67° F (the temperature at high altitudes where compressibility effects in air-cooled engines may become critical), the effect of the free-stream Mach number M on the local heat-transfer coefficient h_x is given by

$$h_x \cong h_{x_i} (1 + 0.056 M^2)$$

where h_{x_i} is the local heat-transfer coefficient that would exist with an incompressible fluid. The effect will be slightly less than shown in the foregoing equation for two reasons: (1) the value h_{x_i} is proportional to the local skin-friction coefficient, which in reference 12 is shown to decrease slightly with increase of Mach number; (2) the highest possible value of $M^2 = 1$ will not exist over the entire cylinder. In practical cases M^2 will not be unity at any point around the cylinder. Consequently, the effect of compressibility on heat-transfer coefficients for the cylinder can be expected to be negligible.

APPARATUS AND TESTS

Test Setup

The copper-plated steel barrel section used in the tests was $1\frac{7}{8}$ inches long with a $5\frac{3}{4}$-inch bore. The fins on the cylinder were 0.50 inch wide, 0.036 inch thick, and spaced 0.105 inch. Inside the cylinder was a grate to aid the pickup of heat and to reduce the temperature variation around the inside of the cylinder. A metal baffle with a 6-inch tailpiece was fitted around the cylinder (fig. 1). The tailpiece allowed the cross flow at the back of the cylinder to diminish sufficiently to permit more reliable pressure reading. The cross-sectional area of the exit of the baffle was 1.6 times the free-flow area between the fins. The unit was placed in an asbestos-lined metal box (fig. 4) and sealed at all edges with furnace cement to prevent air leakage.

The source of heat was an oil burner with a capacity of 1 or 2 gallons of oil per hour, depending on the burner nozzle used. A firebrick furnace provided the space for the combustion to be completed before the hot gases came into contact with the cylinder grate. An auxiliary blower was needed with a large nozzle to supply the necessary air for combustion.

The flow of cooling air was created by two compressors used as vacuum pumps and operated in series. Each pump was driven by an 85-horsepower engine. In order to prevent surging and to smooth out the flow of cooling air, large tanks were placed upstream and downstream of the test cylinder. Bleed valves were placed in front of and between the pumps to provide fine control of the air flow. A tank with thin-plate orifices in each end was placed upstream of the test cylinder to measure the quantity of cooling air. A throttle placed between the orifice tank and the upstream surge tank was used to control the pressure of the cooling air in front of the test cylinder. A diagram of the apparatus is shown in figure 5.

Instrumentation

Surface temperatures of the cylinder were obtained at 24 points (fig. 6) by means of insulated 28-gage chromel-alumel thermocouples spot-welded to the steel. The cold junctions of the thermocouples were inserted in a sealed wooden box. The temperature in the box was obtained with an alcohol-in-glass thermometer; the thermocouple potential was measured with a potentiometer. Thermocouples were also used to measure the orifice temperatures and the cooling-air inlet and outlet temperatures. The cooling-air outlet temperature was measured downstream of the baffle tailpiece in an expanded section; it was therefore unnecessary to correct the readings for air velocity. The outlet duct was lagged to prevent heat loss. The accuracy of the temperature measurements was within ±1° F.

Total and static pressures were obtained in the tailpiece and at two stations on the cylinder; a total pressure was obtained immediately in front of the cylinder (fig. 6). The total-pressure tubes of 0.030-inch-diameter steel tubing with a 0.006-inch-diameter hole in the side of each tube were inserted vertically around the cylinder. The static pressures around the cylinder were measured by means of vertical tubes inserted through holes tapped into the fins (fig. 7). Station 2 was at the baffle constriction and station 3' was somewhat behind the baffle-expansion point. Because of the location of the tube, the static-pressure readings for station 3' were not used in the calculations. Also, in view of the small distance between 3' and 3, the reading $p_{3',t}$ was used for $p_{3,t}$. Conventional-type pressure tubes were not used between the fins because it was thought they would block too much of the channel. A rake of conventional total-pressure tubes was used in surveying the total pressure in the tailpiece, and a wall tap was used to measure the static pressure (fig. 1). The pressures were read on vertical water or mercury manometers, depending on the range of pressures being measured.

The very small pressure drops across the thin-plate orifices were measured with a micromanometer.

Tests

Tests were conducted over a range of air flows at several NACA standard density altitudes from 4000 to 33,000 feet simulated at the front of the cylinder. At each altitude, data were obtained with and without heat transfer for Mach numbers ranging from low values to the highest values obtainable with the apparatus. The highest Mach numbers occurred at the baffle exit, but no accurate data were obtained at that station. In the following table are given the ranges of Mach numbers at the baffle entrance M_2 and at the baffle exit M_o; the M_o values were computed on the assumption of no friction up to that point and are therefore lower than the maximum Mach number of the flow system.

Cylinder condition	Density altitude (ft)	M_2	M_o
Without heat transfer	4,000	0.05 to 0.68	0.05 to 0.68
	15,000	.12 to .70	.12 to .70
	23,000	.17 to .68	.17 to .68
	33,000	.18 to .60	.18 to .60
With heat transfer	4,000	.16 to .73	.18 to .77
	14,000	.16 to .67	.17 to .69
	24,000	.21 to .69	.22 to .74
	32,000	.29 to .56	.31 to .59

Pressures and temperatures were recorded only after the test cylinder had practically reached a state of thermal equilibrium. The maximum allowable rate of change of temperature was about 3° F in 5 minutes for the maximum temperature before readings were taken. The cooling-air outlet temperature was read before and after reading the cylinder temperatures and an average of the two air temperatures was used. The two readings in no case differed by more than 2 percent of the temperature rise. Temperatures were read to within 0.4° F and pressures to within 0.01 inch of mercury or water. The accuracy of the pressure readings was limited by the unsteadiness of the engines, which caused pressure fluctuations of as much as 0.1 inch of mercury.

Summaries of the reduced test data and the derived quantities without and with heat transfer are given in tables 1 and 2, respectively. Cylinder temperature-distribution data are available upon request from the NACA.

COMPUTATIONS

From the tests the following quantities were determined:

W, $H_1 + H_2$, p_{1_t}, T_{1_t}, p_2, p_{2_t}, p_{3_t}, p_4, p_{4_t}, T_4, $T_{f_{av}}$, T_b, α, θ_3, A_2, A_3, A_4, A_b, and S_T

where

A_b area of cylinder wall at base of fins, square feet

T_b average wall temperature, °F absolute (arithmetic average of measured temperatures of cylinder at base of fins)

$T_{f_{av}}$ average temperature of cooling surface (fin and barrel surfaces), °F absolute

S_T total heat-transfer surface of cylinder, square feet

From these data, the fictitious exit density ρ_{ex} and the coefficients h, U, $C_{D_{f_i}}$, C_{p_i}, and $a_3 - C_3$ were determined as follows:

Computation of h. - The average surface heat-transfer coefficient h was calculated from the equation

$$h = \frac{H_1 + H_2}{S_T \left(T_{f_{av}} - T_{1_t}\right)}$$

The average temperature $T_{f_{av}}$ of the fin and barrel surface was obtained from the measured surface temperatures by averaging the temperatures with weighting factors proportional to the area elements in which each thermocouple was located.

Computation of U. - The average wall heat-transfer coefficient U was calculated from the following equation

$$U = \frac{H_1 + H_2}{A_b \left(T_b - T_{1_t}\right)} \tag{24}$$

Computation of fictitious exit density ρ_{ex}. - The stagnation pressure at station 3', the mass flow, the exit stagnation temperature, and the cross section at station 3 were used to compute the

static pressure at station 3 by means of figure 2. This pressure and the temperature T_{4_t} are used to compute the density ρ_{ex} by means of the general gas law.

Computation of $C_{D_{f_i}}$. - By the method given in appendix A, $\frac{T_{2_t} - T_{1_t}}{T_{4_t} - T_{1_t}}$ may be computed from the cooling-surface temperature distribution and the over-all rate of heat transfer. On the assumption that $p_{2_t} = p_{1_t}$, ρ_{2_t} and $(\rho V)^2 / p_{2_t} \rho_{2_t}$ were calculated and, from figure 2, ρ_2, p_2, and q_2 were found. From p_{3_t} and $T_{3_t} = T_{4_t}$, the values of ρ_3, q_3, and p_3 were calculated with the aid of figure 2. A value for $C_{D_{f_i}}$ was then computed from equation (5).

Computation of exit coefficients. - The exit coefficients C_3 and a_3 could not be separately determined and the value of $a_3 \frac{}{} C_3$ was consequently calculated from q_3, p_3, and ρ_3 (obtained in the calculation of $C_{D_{f_i}}$) and equation (17). From p_{4_t} and T_{4_t}, figure 2 was used to find the needed values for ρ_4 and p_4.

Computation of $C_{D_{f_i}}$ by estimation of $a_3 \frac{}{} C_3$. - The value of $C_{D_{f_i}}$ was also calculated by the method of reference 5; that is, by estimating the exit-loss coefficient and assuming $p_3 = p_4$ instead of using the measured value of p_{3_t}. Equation (17) was then used to calculate p_3. Also from previous computations p_2, ρ_2, q_2, T', and M_2^2 were known. The chart (fig. 3) was recalculated for constant values of $(p_2 - p_3)/q_2$ instead of for constant values of $C_{D_{f_i}}$. The new chart was used to find the value of ρ' from $(p_2 - p_3)/q_2$, M_2^2, T'; equation (5) was then used to compute $C_{D_{f_i}}$.

Computation of Reynolds number. - Reynolds numbers R were obtained from the formula

$$R = \frac{\rho V d}{\mu}$$

where

d hydraulic diameter of fin passage, feet

μ absolute viscosity of air based on average of average cooling-surface temperature and average cooling-air temperature, slugs per second per foot

Computation of C_{p_i}. - The pressure-loss coefficients C_{p_i} were calculated from the data by means of equation (20), which was used in the equivalent form

$$C_{p_i} = \frac{\left(1 - p_{4_t}/p_{1_t}\right)}{\frac{1}{2}\left[\frac{(\rho V)^2}{p_{o_t}\ \rho_{o_t}}\right]} \frac{p_{1_t}}{p_{o_t}} \frac{\rho_o}{\rho_{o_t}} \sqrt{1 - M_o^2}$$

From the data it was found that ρ_{o_t} should be calculated from p_{1_t} and T_{4_t} and that p_{o_t} should equal p_{1_t} for the best correlation. In the foregoing equation ρ_{o_t} is the stagnation density. The factor $\frac{(\rho V)^2}{p_{o_t}\ \rho_{o_t}}$ was then calculated and, from the value of this factor, $\frac{\rho_o}{\rho_{o_t}}\sqrt{1 - M_o^2}$ was determined from figure 2.

RESULTS AND DISCUSSION

Evaluation of Coefficients

Correlation of heat-transfer coefficients h and U. - The effect of altitude on the heat-transfer coefficients h and U is shown in figures 8 and 9. The curve for h, the surface heat-transfer coefficient, plotted against weight flow of air at the baffle entrance shows no effect due to altitude inasmuch as the curves for 4000 and 14,000 feet bracket the spread of the data. The curve for U, the wall heat-transfer coefficient, shows the same characteristics as the curve for h. These figures show that the Mach number had no effect on the heat transfer for the range covered. An effect of heat load was noted in the data but is not shown in figures 8 or 9. The heat-transfer coefficients h and U increase slightly with heat-transfer load.

Correlation of pressure-loss function $(\Delta p\ \rho_{av})/\frac{1}{2}(\rho V)^2$. - The pressure-loss function $(\Delta p\ \rho_{av})/\frac{1}{2}(\rho V)^2$ is a dimensionless form of the conventional pressure-loss function $\Delta p\ \rho_{av}/\rho_s$. The density ρ_{av} is the average of densities upstream and downstream of the cylinder, and ρ_s is the air density under standard sea-level conditions. When $(\Delta p\ \rho_{av})/\frac{1}{2}(\rho V)^2$ is plotted against weight flow $\rho V g$ as in figure 10, the conclusions drawn from the plot of the pressure-loss function may be applied to the function $\Delta p\ \rho_{av}/\rho_s$. The dimensionless form has the advantage of showing compressibility effects more clearly.

The plot of the pressure-loss function $\Delta p\ \rho_{av}/\frac{1}{2}(\rho V)^2$ is shown in figure 10 for runs with and without heat transfer. These curves show disagreement for different altitudes and for a variation in heat transfer. The rise shown on the high weight-flow region of each curve indicates an additional pressure loss caused by compressibility effects at high Mach numbers. The high Mach numbers occur at lower weight flows as the density altitude increases. Any correlation method must make it possible to correct for these pressure rises and the separation of the curves for different altitudes and rates of heat transfer.

Correlation of pressure-loss function $(\Delta p\ \rho_{ex})/\frac{1}{2}(\rho V)^2$. - Some investigators have proposed correlating the pressure loss by means of the function $\Delta p\ \rho_{ex}$, where ρ_{ex} is the air density at the exit of the cylinder. This method was unsuccessfully tried with the data of the present tests. In most cases where this method would be applied, the baffle exit would have no tailpiece and consequently no pressure recovery at the baffle exit. The exit density would then be computed from the static pressure at the baffle exit and the stagnation temperature at the tailpiece. The density thus computed is lower than any density existing in any part of the test rig used for the present tests. The pressure-loss function $(\Delta p\ \rho_{ex})/\frac{1}{2}(\rho V)^2$ was computed by means of the density ρ_{ex} and is plotted in figure 11 for tests with and without heat transfer. Because ρ_{ex} decreases as compared with ρ_{av} for increasing pressure losses, the correlation of the pressure-loss function $(\Delta p\ \rho_{ex})/\frac{1}{2}(\rho V)^2$ is better than that of $(\Delta p\ \rho_{av})/\frac{1}{2}(\rho V)^2$. Although the correlation of the runs with heat transfer (fig. 11(b)) is good, the runs without heat transfer (fig. 11(a)) show compressibility effects in that the data for the different density altitudes form separate curves.

Correlation of drag coefficients and exit-recovery coefficients. - The drag coefficients $C_{D_{f_i}}$ computed from the test data by the method previously given are plotted in figure 12 against the weight flow per unit area. The utter lack of correlation between the results for the tests without heat transfer (fig. 12(a)) and those with heat transfer (fig. 12(b)) or between results at different altitudes is evident. The same result is to be observed in figure 13 in which the exit-recovery coefficient $a_3 - C_3$ has been plotted against the cooling-air weight flow.

In order to find the source of error in these results, the assumptions involved in this method were examined. With regard to the assumption that the total pressure remains unchanged between

stations 1 and 2, the data indicated that the pressure drop is so small as to be negligible; at high flows the pressure drop amounts to about 1 percent of the total-pressure loss.

The mass flow was calculated from the total and static pressures at stations 2 and 3' to test the validity of the assumption that the flow is uniform across each section (one-dimensional flow). The calculation was made from the factor $(\rho V)^2/p_t\,\rho_t$, which was obtained from the pressure ratio p/p_t and figure 2. The ratios of the weight flows to the weight flows calculated from measurements at the orifice are plotted for stations 2 and 3' in figures 14 and 15, respectively, against the weight flows obtained from the orifice measurements. At station 2, figure 14 shows that the ratio is near enough unity for application of the assumption of uniform flow. At station 3', however, figure 15 indicates that the measurements are not accurate at low flows. In the calculation of any coefficient based on measurements at one point at station 3', correlation will probably not be obtained. It is partly for this reason that $C_{D_{f_i}}$, as plotted in figure 12, shows such lack of correlation.

In order to eliminate the use of these inaccurate measurements, $C_{D_{f_i}}$ was recalculated by the use of an assumed exit loss instead of the measured loss. The value of a_3 compensates to some extent for the fact that $\theta_3 \neq 90°$. If $a_3 + 2\frac{A_3}{A_4}\sin\theta_3$ is assumed constant for various values of θ_3, then for $\theta_3 = 90°$ separation from the cylinder rear can be expected and no pressure recovery due to pressure gradients along the wall will result. In that case $a_3 = 0$. Then,

$$a_3 + 2\frac{A_3}{A_4}\sin\theta_3 = 2\frac{A_3}{A_4}$$

or

$$a_3 = 2\frac{A_3}{A_4}(1 - \sin\theta_3) \tag{25}$$

If it is further assumed that $C_3 = 0$ and $\rho_3 = \rho_4$ and if $q_3 = q_4\,(A_4/A_3)^2$ is substituted in equation (17), then

$$\frac{p_3 - p_4}{q_4} = -2\,(A_4/A_3 - 1)$$

This equation applies with an incompressible fluid flowing through the sudden expansion of a straight duct.

The method of calculating $C_{D_{f_i}}$ when this loss is used has been previously given. The results are plotted in figure 16. Much better correlation results than was obtained in figure 12, especially at low flows. The data for each altitude form a smooth curve. The curves separate, however, as soon as the Mach number, which increases with altitude for a fixed Reynolds number, becomes appreciable, indicating that the effect of compressibility has been overestimated by taking too high a loss at the exit; that is, a_3 is too low.

In order to determine how much these irregularities in $C_{D_{f_i}}$ and $a_3 - C_3$ affect the over-all total-pressure drop, the values of $C_{D_{f_i}}$ and $a_3 - C_3$ determined from the tests were used to calculate the loss in total pressure to be expected with an incompressible fluid by assuming that the density remains unchanged in all equations for pressure loss. If all losses are added and if ρ = constant = ρ_2,

$$C_{p_i} \equiv \frac{\rho_2 \Delta p_i}{\frac{1}{2}(\rho V)^2} = 1 + C_{D_{f_i}} + C_3 - a_3 - 2\frac{A_3}{A_4} \sin \theta_3 + \left(\frac{A_3}{A_4}\right)^2 \qquad (26)$$

The over-all pressure-loss coefficient C_{p_i} is plotted against the weight flow per unit area in figure 17, which shows that the extreme scatter of the data points in figures 12 and 13 has been sufficiently reduced to allow fairing of curves through the data points. The effect of compressibility may be seen from the fact that the curves show systematic differences for the different altitudes although the ends of the curves do not have the sharp curvature that is evident in the plots of $(\Delta p\ \rho_{av})/\frac{1}{2}(\rho V)^2$. These differences are much smaller than the entire compressibility effect, as may be seen by comparison with figure 10, which is already somewhat corrected for compressibility effects. This result would seem to indicate that, for correction of the compressibility effect, the division of the pressure loss between the baffle channel and the baffle exit is unimportant because the pressure p_3 was no doubt in error. In order to investigate this hypothesis, the over-all pressure-loss coefficient C_{p_i} was computed from the estimated value for $a_3 - C_3$ (equation (25)) and the corresponding values for $C_{D_{f_i}}$ (fig. 16). The results of these calculations are plotted in figure 18, which shows that the value for p_3 cannot be estimated in an arbitrary fashion.

If the values of $C_{D_{f_i}}$ and $a_3 - C_3$ from equations (5) and (17) are inserted in equation (26) in order to determine how the pressure-loss coefficient C_{p_i} depends on the data, there is obtained

$$C_{p_i} = 1 + \left[\frac{2\rho_3}{\rho_3 + \rho_2}\right]\left[\frac{p_2 - p_3}{q_2} - 2\left(\frac{\rho_2}{\rho_3} - 1\right)\right] + \frac{p_3 - p_4}{q_3} + 2\left(\frac{A_3}{A_4}\right)^2\left(1 - \frac{\rho_3}{\rho_4}\right) - \left(\frac{A_3}{A_4}\right)^2 \quad (27)$$

If the density ratios are estimated from the energy equations for very low Mach numbers ($M = 0$), then

$$C_{p_i} = 1 + \left(\frac{p_2 - p_4}{q_2}\right)\left(\frac{1}{1 + \frac{T'}{2}}\right) + \frac{p_4 - p_3}{q_2}\left[\frac{\frac{T'}{2}}{(1 + T')\left(1 + \frac{T'}{2}\right)}\right] - \left(\frac{A_3}{A_4}\right)^2 - \frac{2T'}{1 + \frac{T'}{2}}$$

The value of T' (see equation (8)) is always less than 0.10 and the data indicate that the term involving p_3 is never greater than 0.01. At low Mach numbers, therefore, large variations in estimates of p_3 from its true value will not affect C_{p_i}. For high Mach numbers, however, equation (27) indicates that p_3 will definitely affect the result for C_{p_i}. Figure 15 shows that the measurements of p_3 are inaccurate at low Mach numbers but much better at high Mach numbers; therefore, at high Mach numbers when the data for p_3 are used, fair correlation of C_{p_i} may be expected. At low Mach numbers, the inaccurate values for p_3 do not affect the result; correlation may consequently also be expected in this range. With inaccurate values for $C_{D_{f_i}}$ and $a_3 - C_3$ at low Mach numbers, correlation for C_{p_i} may be expected; whereas, in the high range, correlation may be expected only when accurate values for $C_{D_{f_i}}$ and $a_3 - C_3$ are obtained.

Figure 12(a) shows that no correlation of $C_{D_{f_i}}$ occurs at low Mach numbers and fair correlation occurs at high Mach numbers. No accurate correlation in any range is obtained for tests with heat transfer (fig. 12(b)) but, if scatter is taken about a mean curve for the high Mach numbers, the variations are small compared with the value of C_{p_i} and therefore do not show up so prominently. The same general features of the $C_{D_{f_i}}$ plots (fig. 12) may be observed in the $a_3 - C_3$ plots (fig. 13) and the same comments apply. From the $C_{D_{f_i}}$ data (fig. 16) it may be presumed that the estimate of a_3 was incorrect and resulted in the calculation of faulty values for p_3. Comparison of C_{p_i} of figure 17 with that of figure 18 indicates that, in the range of low Mach numbers for all altitudes, the C_{p_i} curves are the same with the measured and the calculated values of p_3, which confirms the deduction that, for low values of Mach number, C_{p_i} is independent of p_3. In fact, the lowest-altitude curve is approximately

the same for both methods of computing C_{p_i} except at the very highest Mach numbers. The lack of correlation of the data of figure 18 at high Mach numbers confirms the deduction that the estimated values of p_3 are incorrect and influence the values for C_{p_i} and that the measured values for high Mach numbers used in calculating C_{p_i} (fig. 17) are accurate.

The fact that the pressure measurements in the rear of the cylinder were very inaccurate at the low cooling-air weight flows indicates a lack of uniformity in the flow, which contradicts the hypothesis upon which the flow analysis was built. A second inaccuracy is seen in the hypothesis by which $C_{D_{f_i}}$ is calculated from C_{D_f}. The method of calculations is based on the assumption that $q = \frac{1}{2}\rho V^2 = \frac{1}{2}\left[\frac{(\rho V)^2}{\rho}\right]$ increases linearly along the channel; $\frac{1}{2}(q_3 + q_2)$, therefore, represents a good mean value for q. This assumption is approximately true for low Mach numbers but not for high Mach numbers where a much more rapid rate of increase is to be expected. Because $\frac{1}{2}(q_2 + q_3)$ is higher than the mean effective value of q in the channel, $C_{D_{f_i}}$ must be lower than the coefficient that may be expected with a truly incompressible fluid. The nonuniformity of flow in the rear (station 3) will also modify the momentum equations for the baffle channel and the baffle exit. For these reasons values of $C_{D_{f_i}}$ and $a_3 - C_3$ obtained by the assumption of uniform flow and by means of equations (5) and (17) will probably not check estimates from measurements of the velocity and pressure distribution along the channel and baffle walls. Further experiments are required to determine conclusively the effectiveness of this method.

Correlation of the coefficient C_{p_i} calculated by empirical method. - A plot of the pressure-loss coefficient C_{p_i} against the Reynolds number is shown in figure 19. Although the correlation shown in this plot is satisfactory, some features show that improvement is still desirable. The points for the lowest density altitude without heat transfer are, in general, lower than the average of the points. The tendency for this plot to fall off at high Reynolds numbers indicates that the correction for compressibility effects is probably too large. This result might possibly be due to the fact that the correction factor applied is too large for the pressure losses occurring before station 3. This effect does not occur in the data for other density altitudes, possibly because the data for the lowest densities may be inaccurate in the high-flow region as a result of the unsteadiness of the driving engines.

In order to determine the magnitude of these deviations on the actual pressures, the corrected pressure drops were plotted in figure 20 in the customary manner. The discrepancies noted in figure 19 show little effect on the pressure-loss plot. The shape of the plots of figure 19 indicates that a linear curve of pressure-loss data is not to be expected.

General Discussion

Comparison of the correlation methods. - For any set of pressure-loss data, the separation of the curves for different density altitudes is an effect of compressibility that has not been corrected. The effect of compressibility is accentuated at the highest weight flow for each density-altitude curve. The effectiveness of each method of pressure-drop correlation is characterized by the magnitude of the spread of the curves at the four weight flows that are the maximums for the different altitude curves. At the end points of the curves for 4000-, 14,000-, 24,000-, and 32,000-feet density altitudes, there are, respectively, two, four, six, and eight points on all the curves for comparison. The average deviation from the mean of all the curves at these points is given in the following tables in percentage of the mean value of the parameter at that point:

Weight flow (lb/(sec)(sq ft))	Mean deviation, percent		
	Method		
	$\Delta p\ \rho_{av}/\frac{1}{2}(\rho V)^2$	$\Delta p\ \rho_{ex}/\frac{1}{2}(\rho V)^2$	Analytical
14.4	13	7.3	7.8
21.5	13	3.9	4.7
29.0	11	2.8	5.0
40.0	13	4.9	2.1

Reynolds number, R	Mean deviation, empirical method (percent)
0.14×10^5	4.8
.21	2.4
.30	2.1
.40	1.5

These tables show that the use of the variable $(\Delta p\ \rho_{av})/\frac{1}{2}(\rho V)^2$ is least effective, that the use of the variable $(\Delta p\ \rho_{ex})/\frac{1}{2}(\rho V)^2$ and the analytical method are better and about equally effective, and that the empirical method using the Prandtl-Glauert factor is most effective and of satisfactory accuracy.

The involved procedure needed for use of the analytical method is a definite drawback. Furthermore, certain information is needed for pressure-loss predictions that is not necessary when the empirical method is used; the relative amount of heat picked up by the air in front of the baffle entrance must be obtained and pressures at the baffle-channel expansion point are required in order to evaluate separately the coefficients $C_{D_{f_i}}$ and $a_3 - C_3$ in the pressure-loss predictions. The testing technique for determining reliable values of p_3 is yet to be developed. Computations made for a modern engine at an altitude of 40,000 feet show that very high Mach numbers occur and that separate values of $C_{D_{f_i}}$ and $a_3 - C_3$ are needed. The method is somewhat simplified, however, when no baffle tailpiece is used, which eliminates pressure recovery at the baffle exit. In that case $p_3 = p_4$, and pressure measurements are therefore unnecessary in the baffle exit.

The same drawback applies to the use of the pressure-loss function $(\Delta p\ \rho_{ex})/\frac{1}{2}(\rho V)^2$; that is, a measurement of the pressure in the baffle exit is required to determine ρ_{ex} unless a baffle is used that gives complete loss of the kinetic energy at the baffle exit. This method of correcting the pressure loss for compressibility effects has a rational basis. If the entire loss is assumed to occur at the baffle exit, if no pressure recovery exists in the baffle tailpiece, and if the air temperature in the baffle exit is assumed equal to that behind the cylinder, $(\Delta p\ \rho_{ex})/\frac{1}{2}(\rho V)^2$ should very nearly account for all compressibility effects by equation (17). If not all the loss in energy occurs at the baffle exit and if some pressure recovery is present there, this method should give good results if most of the pressure loss occurs at the baffle exit and if the rest varies in much the same manner as the baffle-exit loss.

The empirical method of computation of the pressure loss has the advantage of being quite simple. There is doubt as to the types of flow apparatus to which the empirical method can be applied because no rational basis for it exists at present. Test data from engines, engine cylinders, and radiators are required before an estimate of the reliability of this method can be made. The same confirmation of

the reliability of the analytical method is needed, however, because there is some doubt that it correctly represented the actual flow conditions in even this comparatively simple type of flow path.

In order to illustrate the application of the empirical method, an example is computed and plotted in figure 21. For comparison, the pressure loss is also computed by means of the function $(\Delta p\ \rho_{av})/\frac{1}{2}(\rho V)^2$. The barrel temperature is assumed constant at 350° F; the rate of heat transfer is assumed constant and such as to require an air-weight flow at sea level of 18.5 pounds per second per square foot of free-flow area of the barrel-baffle channel. The atmospheric pressures and temperatures are modified for isentropic compression corresponding to a flight speed of 200 miles per hour. The subsequent steps are:

1. Compute cooling-temperature differential $T_b - T_{l_t}$

2. Compute the heat-transfer coefficient U (equation (24))

3. Determine ρVg (fig. 9); compute the exit temperature

4. Compute the Reynolds number, and determine C_{p_i} (fig. 19)

5. Compute the abscissa of figure 2 and read the compressibility-correction factor $\left(\rho_o/\rho_{o_t}\right)\sqrt{1 - M_o^2}$

6. Compute the pressure loss from the data of steps 3, 4, and 5

When the pressure loss is computed by means of the function $(\Delta p\ \rho_{av})/\frac{1}{2}(\rho V)^2$, the first three steps are the same as those previously given. The weight flow is used to determine $(\Delta p\ \rho_{av})/\frac{1}{2}(\rho V)^2$ by means of the plot of lowest density altitude (fig. 10(b)). An estimate of Δp is made for determining ρ_{av}; the resulting value of Δp is used to refine the values for ρ_{av} and Δp. For less extreme cooling conditions, the difference between the two methods is not so great.

Effect of viscosity. - For the general correlation of pressure-loss and heat-transfer data, dimensionless parameters should be used. The variable h, for example, should be plotted in terms of the Stanton number $\frac{h}{c_p \rho V}$ against the Reynolds number. In turbulent flow the Stanton number varies approximately as the viscosity to the 1/5 power. For practical application of heat-transfer data to altitude-cooling predictions, therefore, the small variation in the

viscosity caused by the variations in temperature of the cooling-air surface film will affect the heat transfer only slightly. Good correlation of heat-transfer data of a given engine or cylinder can be expected, therefore, if the weight flow is used as the correlation variable. The same reasoning can be applied to pressure-loss data. Because the present pressure-loss data were obtained with and without heat transfer, considerable difference should be expected in the film viscosity. Consequently, the Reynolds number was used to correlate the pressure-loss data; the viscosity of the surface film gave better correlation than the cooling-air viscosity in the computation of the Reynolds number. The pressure-loss coefficients were plotted against the weight flow because use of the Reynolds number effected no increase in correlation or significant change in the plot.

Velocity distribution. - Some improvement might be made in the analysis of flow in radiators, for which the assumption of uniform flow at the radiator-tube exit is satisfactory, if allowance were made in the momentum equation for the nonuniformity of flow to be expected with a turbulent velocity distribution in the tube. The computed kinetic-energy loss at the exit would thus be increased.

SUMMARY OF RESULTS

Based on an analysis of pressure-drop requirements and on experiments to determine the effect of air compressibility on cooling and pressure loss of a baffled cylinder barrel, the following results were obtained:

1. The pressure loss from the front of the cylinder to the baffle entrance was very small, as might be expected for any baffled engine cylinder.

2. The method of analyzing the flow processes around a baffled cylinder based on the assumption of uniform flow corrected for most of the effect of compressibility.

3. The assumption of uniform flow used in the analytical method of predicting pressure losses was not verified by computations from pressure measurements between the fins at low flows.

4. Prediction of the pressure losses across a cylinder at high Mach numbers using the analytical method based on uniform flow requires knowledge of the exact values of the friction coefficient between the fins and the coefficient at the exit of the cylinder. At low Mach numbers the division of the pressure coefficients has little effect on predicted pressure loss.

5. The use of a fictitious exit density ρ_{ex} in correcting pressure-loss data gives as accurate correlation as the analytical method based on the assumption of uniform flow.

6. An empirical method has been found which gives satisfactory correlation (mean deviation of pressure-function curves of about 3 percent) of the test data on pressure loss of the present cylinder and which permits estimates to be made of compressibility and heating effects more simply than either the analytical method or the method using the baffle-exit density in baffle-flow systems with a tailpiece.

CONCLUSION

If engine-cooling equations are based on the cooling-air weight flow instead of on the pressure loss, good correlation of data and prediction of performance may be expected because test data and theoretical estimates showed no appreciable effect of air compressibility on heat-transfer coefficients in the ordinary range of engine operating conditions.

Aircraft Engine Research Laboratory,
National Advisory Committee for Aeronautics,
Cleveland, Ohio.

APPENDIX A

ESTIMATION OF AIR-TEMPERATURE DISTRIBUTION AROUND A BAFFLED CYLINDER BARREL

In order to determine the pressure loss over the cylinder, it is necessary to know the rate of heat transfer to the cooling air between stations 1 and 2 H_1 and the rate of heat transfer to the cooling air in the baffled section H_2. The following analysis presents one method of estimating H_1 and H_2.

For an element of heat-transmitting surface dS, the amount of heat transferred per unit time is

$$dH = h_x (T_f - T_t)\, dS \tag{A1}$$

where

H rate of heat transfer from front of cylinder to point being considered, Btu/sec

h_x local surface heat-transfer coefficient, Btu/(sec)($^{\circ}$F)(sq ft)

T_f cooling-surface temperature average at any local flow section, $^{\circ}$F absolute

T_t local stagnation-air temperature, $^{\circ}$F absolute

The viscous shearing stress slows down the air in the immediate vicinity of the wall and increases the temperature there until T, the temperature upon which the heat transfer depends, is more properly the stagnation temperature than the static temperature (reference 11). If W_L is the local weight flow between the fins (lb/sec), the energy equation is

$$H = c_p W_L (T_t - T_{1t}) \tag{A2}$$

In the unbaffled section of the cylinder, W_L increases from a value of zero at the front stagnation point to the value W at the baffle entry. The term T_t is eliminated from equations (A2) and (A1) and the quantities

$$C \equiv \frac{h_x S_T}{c_p W_L}$$

and

$$t \equiv T_f - T_{l_t} = \text{cooling-temperature differential, } {}^{\circ}F$$

are used to obtain

$$dH = C\,(c_p W_L t - H)\,d(S/S_T)$$

where

S_T entire surface for heat transfer, sq ft

S surface for heat transfer from front of cylinder to point considered, sq ft

The solution of this differential equation is

$$H = \exp\left[-\int_0^{S/S_T} Cd(S/S_T)\right]\left\{\text{Constant} + \int_0^{S/S_T} Cc_pW_Lt\exp\left[\int_0^{S/S_T} Cd(S/S_T)\right]d(S/S_T)\right\} \quad (A3)$$

Because $S/S_T = 0$ and $H = 0$ at the front of the cylinder, the constant of integration is zero. At the baffle entry, S/S_T is equal to a, the ratio of the unbaffled cooling surface of the cylinder to the total cooling surface, and $H = H_1$, the rate of heat exchange in the unbaffled portion of the cylinder. At the baffle exit, $S/S_T = 1$, and $H = H_1 + H_2$, the rate of heat exchange over the entire cylinder. When these boundary conditions are inserted in equation (A3),

$$H_1 = \exp\left[-\int_0^a Cd(S/S_T)\right]\int_0^a Cc_pW_Lt\exp\left[\int_0^{S/S_T} Cd(S/S_T)\right]d(S/S_T) \quad (A4)$$

$$H_1 + H_2 = \exp\left[-\int_0^1 Cd(S/S_T)\right]\int_0^1 Cc_pW_Lt\exp\left[\int_0^{S/S_T} Cd(S/S_T)\right]d(S/S_T) \quad (A5)$$

The rest of this appendix derives expressions for H_1 and $H_1 + H_2$, which are more convenient than equations (A4) and (A5) for computation from the test data. The quantity C varies little over

the cylinder except at the very front. The factor $e^{\int_0^{S/S_T} Cd(S/S_T)}$ and the integral of $CW_L te^{\int_0^{S/S_T} Cd(S/S_T)} d(S/S_T)$ are only slightly affected by this variation. Consequently, the quantity C is considered a constant in all the integrations. The values found for H_1 and $H_1 + H_2$ from the energy equations

$$H_1 = Wc_p \left(T_{2_t} - T_{1_t}\right)$$

and

$$H_1 + H_2 = Wc_p \left(T_{4_t} - T_{1_t}\right)$$

are substituted in equations (A4) and (A5) to obtain

$$T_{2_t} - T_{1_t} = C\, e^{-C\alpha} \int_0^{\alpha} \frac{W_L}{W}\, t\, e^{C(S/S_T)}\, d(S/S_T) \qquad (A6)$$

$$T_{t_4} - T_{t_1} = Ce^{-C}\left[\int_0^{\alpha} \frac{W_L}{W}\, te^{C(S/S_T)}\, d(S/S_T) + \int_{\alpha}^{1} \frac{W_L}{W}\, te^{C(S/S_T)}\, d(S/S_T)\right] \qquad (A7)$$

$$T_{t_4} - T_{t_1} = e^{-C(1-\alpha)}\left(T_{2_t} - T_{1_t}\right) + Ce^{-C}\int_{\alpha}^{1} \frac{W_L}{W}\, te^{C(S/S_T)}\, d(S/S_T) \qquad (A8)$$

If an estimate is made of the weight-flow variation W_L/W and measurements of t are obtained, C can be determined from the over-all temperature rise $T_{4_t} - T_{1_t}$ and equation (A7) and its value used in equation (A6) to find $T_{2_t} - T_{1_t}$.

In order to estimate the weight-flow variation in the unbaffled portion of the cylinder, the flow in the front is computed by means of the equation for potential flow over a circular cylinder. The velocity over such a cylinder is

$$V = 2\, V_o \sin \pi\, (S/S_T)$$

where V_o is the velocity of the undisturbed flow, which reaches a maximum at $S/S_T = 1/2$. In the case of the baffled cylinder the

maximum value is at $S/S_T = a$. The velocity function is therefore modified to take this factor into account

$$V = 2 V_o \sin (\pi S/2a S_T)$$

The constriction at the baffle entrance $(S/S_T = a)$ of the flow area to $1/n$ its value for an unbaffled cylinder increases the maximum velocity by the factor n, but the velocity in front of the cylinder is unchanged. The velocity distribution must therefore be multiplied by an even function of S/S_T, which increases from a value of 1 at $S/S_T = 0$ to a value of n at $S/S_T = a$. The assumed function is $n\left[1 - \frac{n-1}{n} \cos (\pi S/2a S_T)\right]$ which gives an approximate weight-flow variation of

$$\frac{W_L}{W} = \sin (\pi S/2a S_T) - \frac{n-1}{2n} \sin \frac{\pi}{a} (S/S_T) \qquad (A9)$$

From the baffle dimensions, $n = 5$. For the unbaffled portion of the cylinder, a linear cooling-surface temperature distribution is assumed

$$t/t_2 = t_1/t_2 - \left(\frac{t_1 - t_2}{t_2}\right)\frac{S/S_T}{a} \qquad (A10)$$

where t_1 is the value of t at $S/S_T = 0$, and t_2 is the value of t at $S/S_T = a$. Equations (A9) and (A10) are substituted in equation (A6) to obtain

$$\left(T_{2_t} - T_{1_t}\right)\Big/ t_2 = f_1 (C) + \left(\frac{t_1 - t_2}{t_2}\right) f_2 (C) \qquad (A11)$$

where

$$f_1(C) \equiv \frac{C}{C^2 + \left(\frac{\pi}{2a}\right)^2}\left[C + \frac{\pi}{2a} e^{-Ca}\right] - \frac{n-1}{2n} \frac{C}{C^2 + \left(\frac{\pi}{a}\right)^2} \frac{\pi}{a} \left(1 + e^{-Ca}\right)$$

$$f_2(C) \equiv \frac{C}{\alpha\left[C^2 + \left(\frac{\pi}{2\alpha}\right)^2\right]^2}\left\{C^2 - \left(\frac{\pi}{2\alpha}\right)^2 + e^{-C\alpha}\,\pi\left[C/\alpha + \frac{1}{2}\left(C^2 + \left(\frac{\pi}{2\alpha}\right)^2\right)\right]\right\}$$

$$- \frac{\frac{n-1}{2n}\,C}{\alpha\left[C^2 + \left(\frac{\pi}{\alpha}\right)^2\right]^2}\left\{2C\,\frac{\pi}{\alpha} + e^{-C\alpha}\left[2C\,\frac{\pi}{\alpha} + \pi\left(C^2 + \left(\frac{\pi}{\alpha}\right)^2\right)\right]\right\}$$

An approximation must now be found for the integral involved in equation (A8). In the baffled section $W_I/W = 1$ and t varies very little; an extreme case shows 9-percent average deviation from the mean. The unbaffled cylinder rear shows a much larger deviation but the decrease in the effective cooling-air velocity reduces the variation of the function $(W_L/W)\,t$. The value of W_L/W is therefore taken to be unity and an average value used for t so that

$$\int_{\alpha}^{1} \frac{W_L}{W}\,t\,e^{C(S/S_T)}\,d\,(S/S_T) = \frac{1}{C}\left[e^{C} - e^{C\alpha}\right]\,t_3 \qquad (A12)$$

where t_3 is the average cooling-surface temperature of the cylinder from the baffle entrance to the rear minus the inlet-air temperature. This result is substituted in equation (A8) to obtain

$$\left(T_{2_t} - T_{1_t}\right) = \left(T_{4_t} - T_{1_t}\right) - \left[t_3 - \left(T_{4_t} - T_{1_t}\right)\right]\left[e^{C(1-\alpha)} - 1\right] \qquad (A13)$$

If

$$t_a \equiv \frac{1}{2}\left(t_2 + t_1\right)$$

equation (A11) can be plotted in the form $\left(T_{2_t} - T_{1_t}\right)/t_a$ is a function of $\left[\left(e^{C(1-\alpha)} - 1\right)\right.$ and $\left.\left(t_1 - t_2\right)/t_a\right]$. This plot is shown in figure 22. Equation (A13), however, gives a solution for the variable $\left(T_{2_t} - T_{1_t}\right)/t_a$ as a linear function of $e^{C(1-\alpha)} - 1$ with a y intercept of $\left(T_{4_t} - T_{1_t}\right)/t_a$ and a slope of

$\left[t_3 - \left(T_{4_t} - T_{1_t}\right)\right]/t_a$. From data on the temperature of the cylinder, the straight line (equation (A13)) can be located on figure 22 and the intersection point can be obtained with the curve of equation (A11) for the proper value of $(t_1 - t_2)/t_a$; thus, $\left(T_{2_t} - T_{1_t}\right)/t_a$ can be determined.

APPENDIX B

SYMBOLS

$$a_3 \equiv \int \frac{(p - p_3)\, dS_x}{\frac{1}{2} \rho_3 V_3^2 A_4}$$

A cross-sectional area at a station indicated by a subscript (except with subscript b), sq ft

A_b area of cylinder wall at base of fins, sq ft

c_p specific heat of air at constant pressure, Btu/(lb)(°F)

$C = \frac{(h_x S_T)}{(c_p W_L)}$

C_3 coefficient for friction drag in baffle exit

C_{D_f} coefficient for skin-friction drag from station 2 to station 3 based on dynamic pressure at station 2

$C_{D_{f_i}}$ coefficient for drag from station 2 to station 3 based on dynamic pressure averaged in baffle channel

C_{p_i} pressure-loss coefficient with an incompressible fluid

C_{p_M} pressure-loss coefficient with a compressible fluid

g acceleration of gravity, ft/sec^2

h_x local surface heat-transfer coefficient, Btu/(sec)(°F)(sq ft)

h average surface heat-transfer coefficient, based on inlet-air temperature, Btu/(sec)(°F)(sq ft)

H rate of heat transfer from cylinder area between front and any point considered, Btu/sec

H_1 rate of heat transfer to air from front of cylinder to baffle entry, Btu/sec

H_2 rate of heat transfer from baffle entry to baffle exit (station 2 to station 4), Btu/sec

M Mach number at a station indicated by subscript (except M_a, M_b)

$$M_a = \sqrt{\frac{\rho' - 1}{\gamma\rho'\left[\frac{C_{Df_i}}{4}(1 + \rho') + (\rho' - 1)\right] + \frac{\gamma - 1}{2}(1 - \rho'^2)}}$$

$$M_b = \frac{M_a}{\sqrt{\rho' - 1}}$$

p static or stagnation (indicated by subscript t) pressure at any point in fluid indicated by a subscript, lb/sq ft

p_i static pressure at any point in fluid with incompressible flow, lb/sq ft

q dynamic pressure at any point in fluid indicated by subscript, lb/sq ft

R Reynolds number

S surface for heat transfer from front of cylinder to point considered, sq ft

S_T total heat-transfer surface of cylinder, sq ft

S_x projected area of cylinder-wall surface or curved part of baffle surface back of station 3 on plane of A_4, sq ft

$t \equiv T_f - T_{l_t}$

$t_a \equiv \frac{1}{2}(t_2 + t_1)$

t_3 average value of t between stations 2 and 4, °F

T true air-stream or stagnation (indicated by subscript t) temperature at any point in fluid indicated by subscript (except T_b, T_f, and $T_{f_{av}}$, °F absolute

T_b average temperature of cylinder wall at base of fins, °F absolute

T_f cooling-surface temperature averaged at any local flow section, °F absolute

$T_{f_{av}}$ average temperature of cooling surface of cylinder, °F absolute

$T' \equiv H_2/c_p\, WT_2$

U wall heat-transfer coefficient of cylinder, Btu/(sec)(sq ft) ($^\circ$F)

V velocity of air at any station indicated by subscript, ft/sec

W weight of air flowing through baffle, lb/sec

W_L local air weight flow between fins, lb/sec

α ratio of unbaffled cooling surface of cylinder to total cooling surface

γ ratio of specific heats for air (1.3947)

θ_3 angle between radii of cylinder to cylinder rear and to station 3, deg (See fig. 1.)

μ absolute viscosity, slugs/(sec)(ft)

ρ local true or stagnation (indicated by subscript t) density at any point indicated by subscript (except ρ_s, ρ_{av}, and ρ_{ex}), slugs/cu ft

ρ_s standard density of air at 29.92 in. Hg and 60° F, slugs/cu ft

ρ_{av} average of densities at stations 1 and 4, slugs/cu ft

ρ_{ex} fictitious exit density

$\rho' \equiv \rho_2/\rho_3$

Δp total-pressure drop from front to rear of cylinder, lb/sq ft or in. water, $\left[p_{1_t} - p_{4_t}\right]$

Δp_i loss in total pressure from front to rear of cylinder with an incompressible fluid, lb/sq ft or in. water

Δp_{i_s} loss in total pressure from front to rear of cylinder with an incompressible fluid under standard density conditions, lb/sq ft or in. water

Subscripts applicable to A, p, T, V, ρ, M, and q:

1, 2, 3, 3', 4 stations indicated in figure 1

t stagnation condition of gas (absence of subscript t indicates true-stream condition)

o condition characteristic of entire flow

REFERENCES

1. Pinkel, Benjamin: Heat-Transfer Processes in Air-Cooled Engine Cylinders. NACA Rep. No. 612, 1938.

2. Pinkel, Benjamin, and Ellerbrock, Herman H., Jr.: Correlation of Cooling Data from an Air-Cooled Cylinder and Several Multicylinder Engines. NACA Rep. No. 683, 1940.

3. Schey, Oscar W., and Pinkel, Benjamin: Cooling of a Radial Engine in Flight. Jour. Aero. Sci., vol. 4, no. 11, Sept. 1937, pp. 448-452.

4. Corson, Blake W., Jr., and McLellan, Charles H.: Cooling Characteristics of a Pratt & Whitney R-2800 Engine Installed in an NACA Short-Nose High-Inlet-Velocity Cowling. NACA ACR No. L4F06, 1944.

5. Becker, John V., and Baals, Donald D.: The Aerodynamic Effects of Heat and Compressibility in the Internal Flow Systems of Aircraft. NACA ACR, Sept. 1942.

6. Meredith, F. W.: Note on the Cooling of Aircraft Engines with Special Reference to Ethylene Glycol Radiators Enclosed in Ducts. R. & M. No. 1683, British A.R.C., 1936.

7. Winter, H.: Contribution to the Theory of the Heated Duct Radiator. NACA TM No. 893, 1939.

8. Weise, A.: The Conversion of Energy in a Radiator. NACA TM No. 869, 1938.

9. Brevoort, Maurice J., Joyner, Upshur T., and Wood, George P.: The Effect of Altitude on Cooling. NACA ARR, March 1943.

10. von Kármán, Th.: Compressibility Effects in Aerodynamics. Jour. Aero. Sci., vol. 8, no. 9, July 1941, pp. 337-356.

11. Frankl, F.: Heat Transfer in the Turbulent Boundary Layer of a Compressible Gas at High Speeds; Frankl, F., and Voishel, V.: Friction in the Turbulent Boundary Layer of a Compressible Gas at High Speeds. NACA TM No. 1032, 1942.

12. Emmons, H. W., and Brainerd, J. G.: Temperature Effects in a Laminar Compressible-Fluid Boundary Layer Along a Flat Plate. Jour. Appl. Mech., vol. 8, no. 3, Sept. 1941, pp. A-105-A-110.

TABLE 1. - SUMMARY OF DATA FOR TESTS WITHOUT HEAT TRANSFER

[The symbols used are defined in appendix B]

NATIONAL ADVISORY COMMITTEE FOR AERONAUTICS

Density altitude (ft)	P_{1_t} (in. Hg abs.)	T_{1_t} (°F abs.)	VP_g (lb/(sec)(sq ft))	$P_{1_t} - P_{4_t}$ (in. Hg)	P_{g_t} (in. Hg abs.)	P_2 (in. Hg abs.)	$P_{3'_t}$ (in. Hg abs.)	$P_{3'}$ (in. Hg abs.)	P_4 (in. Hg abs.)	Δpp_{av} / $1/2(\rho V)^2$	Δpp_{ex} / $1/2(\rho V)^2$	$a_3 - C_3$	$C_{D_{f_1}}$	C_{p_1} (analytical method)	C_{p_1} (empirical method)	Reynolds number x 10^{-5}	ΔP_{1_s} (in. H_2O)
4,000	28.10	542.8	3.892	0.08	28.11	28.04	28.06	28.07	27.95	1.656	1.653	-0.5882	0.2212	1.7116	1.5888	0.0465	0.97
	28.12	542.8	4.030	.07	28.12	28.05	28.21	28.21	28.11	1.353	1.353	-.7491	-.2179	1.4334	1.3422	.0482	.86
	28.19	543.5	4.494	.09	28.20	28.11	28.16	28.16	28.04	1.383	1.381	-.1232	.4762	1.5016	1.3889	.0537	1.10
	28.26	544.5	5.464	.09	28.26	28.15	28.25	28.22	28.11	.934	.933	-.2614	-.1170	1.0466	.9361	.0651	1.09
	28.34	544.5	6.477	.14	28.31	28.18	28.30	28.22	28.12	1.040	1.036	.2093	.3695	1.0624	1.0238	.0772	1.70
	28.20	545.5	7.521	.15	28.19	28.01	28.17	28.06	27.96	.819	.818	.1859	.1074	.8237	.8141	.0894	1.81
	28.11	545.5	9.230	.22	28.11	27.81	28.09	27.87	27.77	.795	.791	.2462	.1134	.7694	.7855	.1097	2.62
	28.14	546.5	11.487	.29	28.13	27.73	28.08	27.76	27.64	.675	.668	.3562	.0900	.6360	.6648	.1362	3.43
	28.20	546.5	13.386	.42	28.25	27.65	28.10	27.64	27.52	.720	.709	.3375	.1489	.7136	.7048	.1584	4.94
	28.24	545.5	15.791	.58	28.23	27.45	28.06	27.40	27.33	.713	.698	.4496	.2107	.6633	.6900	.1876	6.74
	28.16	540.7	18.217	.79	28.15	27.16	27.97	27.09	26.97	.730	.710	.4546	.1701	.6177	.6990	.2190	9.11
	28.16	541.8	19.810	.91	28.16	26.95	27.90	26.82	26.72	.708	.682	.4925	.1890	.5987	.6748	.2377	10.37
	28.14	542.8	22.173	1.12	28.13	26.58	27.82	26.40	26.28	.685	.657	.5329	.1866	.5559	.6430	.2626	12.36
	28.23	543.5	24.673	1.38	28.21	26.41	27.81	26.15	26.05	.679	.643	.5357	.1828	.5493	.6263	.2934	14.90
	28.22	549.2	26.772	1.73	28.21	25.89	27.69	25.54	25.47	.718	.682	.5139	.2001	.5884	.6510	.3176	18.19
	28.23	547.9	29.736	2.22	28.20	25.35	27.62	24.89	24.80	.737	.667	.5112	.1774	.5684	.6482	.3530	22.29
	28.18	548.2	33.375	2.99	28.14	24.36	27.34	23.61	23.99	.769	.670	.5177	.1712	.5557	.6425	.3949	27.98
	28.09	547.0	38.74	4.61	28.08	22.28	27.02	20.99	21.00	.839	.681	.4849	.1600	.5773	.6126	.4456	36.06
	28.11	551.0	40.60	5.14	28.04	21.71	26.97	20.09	20.05	.834	.647	.5040	.1430	.5442	.5561	.4739	35.89
	28.16	557.0	39.75	4.97	28.10	21.89	26.98	20.27	20.27	.837	.665	.4925	.1692	.5789	.5834	.4587	35.90
15,000	20.08	549.0	6.508	.20	20.08	19.84	19.99	20.34	19.73	1.029	1.021	.3018	.4516	1.0520	1.0270	.0771	1.70
	19.95	550.0	7.627	.25	19.94	19.61	19.95	20.14	19.52	.928	.924	-.0606	-.0466	.9162	.9115	.0885	2.08
	20.03	550.0	9.494	.36	20.03	19.55	19.95	20.06	19.45	.865	.853	.2120	.2137	.9069	.8431	.1105	2.98
	19.92	551.0	10.411	.42	19.90	19.34	19.86	19.89	19.23	.832	.818	.1769	.1334	.8587	.8126	.1206	3.43
	20.12	551.0	11.58	.52	----------	18.92	20.00	19.09	19.27	.837	.818	.3114	.2238	.8146	.8101	.1342	4.27
	20.11	544.0	15.79	.91	20.08	18.87	19.88	19.33	18.65	.787	.752	.4213	.2053	.6862	.7449	.1870	7.23
	20.16	549.0	19.46	1.14	20.14	18.20	20.73	19.56	18.88	.637	.622	.0296	-.2511	.6215	.5737	.2260	8.46
	20.12	549.0	22.22	1.62	----------	17.51	20.56	18.74	18.02	.680	.649	.1479	-.1405	.6138	.5839	.2580	11.21
	20.04	549.0	23.74	2.26	20.01	17.04	19.45	17.21	15.91	.811	.716	.4478	.1839	.6383	.6712	.2770	14.87
	20.09	549.0	26.31	2.97	20.06	16.27	20.30	16.16	15.36	.846	.712	.4561	.1923	.6294	.6561	.3060	17.82
	20.16	550.0	28.81	4.12	20.16	15.40	19.23	14.71	13.80	.941	.742	.4362	.1724	.6384	.6554	.3340	21.25
	20.02	555.0	29.08	4.44	20.01	14.92	18.96	13.76	12.76	.965	.712	.4987	.1504	.5539	.6494	.3363	21.37
	20.16	547.6	10.35	.34	20.14	19.57	20.06	20.04	19.39	.695	.682	.4314	.1743	.6451	.6776	.1226	2.83
	20.20	547.6	12.34	.59	20.22	19.44	20.08	19.88	19.26	.842	.823	.3333	.1759	.7448	.8132	.1461	4.85
	20.20	547.6	15.25	.84	20.17	19.01	20.02	19.42	18.81	.777	.747	.3984	.1605	.6643	.7356	.1806	6.69
	20.15	546.6	17.72	1.16	20.14	18.55	19.84	18.88	18.22	.781	.735	.4266	.1963	.6719	.7222	.2100	8.85
	20.24	547.6	19.84	1.40	----------	18.20	19.85	18.46	17.80	.751	.693	.4822	.1888	.6088	.6781	.2350	10.39
	20.16	547.6	24.60	2.43	20.14	16.97	19.47	16.92	16.21	.858	.752	.4456	.1951	.6817	.7179	.2913	16.10
23,000	14.82	552.0	6.93	.30	14.82	14.44	14.71	15.45	14.35	.998	.981	.1846	.3430	1.0606	.9803	.0807	1.84
	15.00	539.6	10.60	.69	15.02	14.20	14.80	15.10	13.99	1.007	.974	.2883	.2688	.8827	.9688	.1285	4.21
	15.07	542.6	12.41	.86	15.06	13.94	14.92	14.84	13.67	.898	.857	.2579	.1416	.7859	.8456	.1492	5.08
	15.01	545.6	15.35	1.33	14.99	13.30	14.72	14.08	12.86	.875	.811	.3570	.1689	.7141	.7848	.1827	7.20
	15.07	546.6	17.75	1.84	15.07	12.76	14.70	13.43	12.13	.890	.791	.3617	.1383	.6788	.7505	.2104	9.23
	14.86	549.0	8.07	.41	14.89	14.38	14.80	15.39	14.27	1.010	.995	.0188	.1703	1.0537	.9736	.0947	2.50
	14.83	549.0	9.18	.47	14.82	14.19	14.73	15.21	14.15	.887	.864	.1877	.2186	.9331	.8603	.1077	2.83
	14.91	550.0	10.09	.56	14.91	14.15	14.83	15.18	14.01	.875	.850	.2572	.2590	.9040	.8304	.1180	3.34
	14.91	550.0	11.68	.74	14.91	13.92	14.78	14.89	13.70	.853	.824	.4615	.1624	.6031	.8037	.1366	4.30
	14.88	550.0	13.86	1.09	14.89	13.51	14.68	14.42	13.16	.877	.828	.3039	.1894	.7877	.8045	.1621	6.02
	14.91	551.0	15.54	1.37	14.89	13.14	14.62	14.03	12.73	.867	.797	.3585	.2094	.7531	.7658	.1813	7.22
	14.90	543.0	18.09	1.97	14.90	12.47	14.44	13.25	11.83	.892	.784	.3948	.1771	.6845	.7379	.2157	9.55
	14.89	549.0	19.21	2.27	14.88	12.06	14.37	12.79	11.76	.901	.772	.3658	.1772	.6942	.7137	.2253	10.33
	14.85	547.0	21.52	3.31	14.84	11.21	14.17	11.34	9.62	.988	.774	.4061	.1521	.6482	.6826	.2551	12.33
33,000	10.77	552.0	5.36	.27	10.76	10.40	10.70	12.02	10.31	1.089	1.072	.0757	.3262	1.1527	1.0690	.0625	1.20
	10.73	552.0	6.39	.34	10.72	10.23	10.60	11.87	10.12	.961	.931	.3279	.3708	.9451	.9263	.0743	1.48
	10.79	553.0	7.39	.47	10.75	10.14	10.62	11.77	9.99	.983	.948	.3390	.3865	.9497	.9391	.0860	2.02
	10.76	552.0	14.46	2.11	10.75	8.35	10.44	9.68	7.25	1.027	.890	.2467	.1540	.8095	.7961	.1683	6.51
	10.70	553.0	13.23	1.71	10.67	8.69	10.38	10.20	7.95	1.017	.902	.2466	.1961	.8517	.8363	.1539	5.75
	10.68	554.0	11.20	1.15	10.67	9.24	10.44	10.88	8.81	.987	.912	.2493	.2231	.8760	.8874	.1300	4.30
	10.72	553.0	9.05	.76	10.70	9.78	10.57	11.44	9.54	1.034	.980	.2995	.3436	.9463	.9619	.1051	3.09

NATIONAL ADVISORY COMMITTEE FOR AERONAUTICS

TABLE 2. - SUMMARY OF DATA FOR TESTS WITH HEAT TRANSFER

[The symbols used are defined in appendix B]

Density altitude (ft)	p_{1_t} (in. Hg abs.)	T_{1_t} (°F abs.)	$V\rho_g$ (lb/(sec)(sq ft))	$p_{1t} - p_{4_t}$ (in. Hg)	T_{4t} (°F abs.)	p_{2_t} (in. Hg abs.)	p_2 (in. Hg abs.)	$p_{3't}$ (in. Hg abs.)	p_3 (in. Hg abs.)	p_4 (in. Hg abs.)	$T_{f_{av}} - T_{1_t}$ (°F)	$T_b - T_{1_t}$ (°F)
4,000	27.80	550.6	12.22	0.54	630.6	27.77	27.27	27.59	27.05	27.02	310.56	367.00
	28.00	551.1	14.97	.70	628.6	27.97	27.24	27.75	26.94	26.96	302.17	365.55
	28.04	552.1	18.16	1.01	623.1	28.03	26.92	27.74	26.50	26.49	283.50	351.15
	28.02	553.1	21.52	1.39	620.6	28.01	26.43	27.64	25.85	25.90	268.39	340.09
	27.99	553.6	26.30	2.12	613.6	27.93	25.56	27.42	24.65	24.77	250.09	321.75
	27.94	555.6	29.53	2.75	611.6	27.93	24.85	27.21	23.46	23.62	238.69	310.63
	28.15	550.1	36.12	4.69	597.1	28.13	23.50	27.06	20.85	21.13	202.06	289.25
	28.09	547.1	39.62	6.76	593.6	28.02	22.13	26.88	17.57	18.08	200.30	273.38
	28.01	553.8	40.85	7.60	594.6	27.96	21.69	26.79	15.86	16.45	180.16	246.21
14,000	20.47	540.4	8.55	.39	615.8	20.48	20.07	20.38	20.61	19.90	234.96	270.46
	20.47	541.0	11.37	.61	606.2	20.44	19.78	20.30	20.28	19.52	217.77	255.09
	20.47	541.3	14.54	.85	597.4	20.44	19.39	20.24	19.84	19.06	198.07	239.09
	20.48	542.1	17.25	1.22	593.2	20.44	18.94	20.12	19.32	18.51	185.02	227.09
	20.42	542.1	19.68	1.64	589.1	20.37	18.38	19.90	18.63	17.79	172.66	217.54
	20.46	542.1	22.31	2.18	585.6	20.45	17.82	19.34	17.42	16.91	166.00	211.17
	20.61	542.1	26.87	3.44	580.9	20.60	16.63	19.74	16.12	15.14	151.53	197.29
	20.53	549.2	29.05	4.61	581.9	--------	16.16	19.47	14.18	13.05	142.12	185.88
24,000	14.98	549.6	8.20	.52	625.6	15.00	14.52	14.80	14.71	14.24	251.15	289.00
	14.97	551.1	11.49	.89	616.1	14.98	14.09	14.67	14.06	13.54	227.34	268.54
	15.03	551.6	15.41	1.43	606.1	14.99	13.44	14.67	13.25	12.76	204.24	246.92
	15.06	556.1	21.52	4.10	602.1	--------	12.26	14.35	9.35	8.75	183.06	227.25
	14.87	557.6	10.09	.77	650.6	14.85	14.13	14.51	14.15	13.65	308.47	360.55
	14.84	557.6	13.96	1.35	632.6	14.82	13.49	14.47	13.34	12.84	263.83	317.38
	14.84	556.6	15.85	1.80	624.6	14.81	13.06	14.33	12.62	12.18	246.77	300.13
	14.92	559.6	18.26	2.41	622.1	14.89	12.56	14.30	11.69	11.19	230.82	287.00
32,000	11.18	537.6	8.55	.60	603.3	11.19	10.36	11.01	12.10	10.08	208.02	240.92
	11.18	539.3	9.76	.92	604.3	11.16	10.11	10.95	11.77	9.67	210.69	245.92
	11.19	539.6	11.37	1.28	600.8	11.16	9.75	10.92	11.36	9.17	201.45	237.46
	11.18	540.4	12.22	1.66	598.9	11.15	9.49	10.86	10.97	8.60	197.11	235.04
	11.18	542.1	14.01	2.22	598.2	11.17	8.99	10.81	10.25	7.67	191.92	231.79
	11.24	542.8	14.37	2.56	598.2	11.25	8.93	10.90	9.96	7.23	189.42	228.96

Density altitude (ft)	U (Btu/(hr)(sq in.)(°F))	h (Btu/(hr)(sq in.)(°F))	t_a (°F)	$\frac{t_1 - t_2}{t_a}$	t_3 (°F)	$\frac{\Delta p \rho_{av}}{1/2(\rho V)^2}$	$\frac{\Delta p \rho_{ex}}{1/2(\rho V)^2}$	$a_3 - c_3$	$c_{p_{f_1}}$	c_{p_1} (analytical method)	c_{p_1} (empirical method)	Reynolds number x10^{-5}	Δp_{1_s} (in. H_2O)
4,000	0.636	0.0861	365.0	0.8055	236.6	1.019	0.931	0.4572	0.2347	0.6797	0.9299	0.1126	5.432
	.758	.1052	359.5	.8372	224.3	.880	.802	.4595	.1612	.6039	.7979	.1385	6.994
	.878	.1246	340.0	.8529	203.5	.863	.780	.4118	.1834	.6738	.7741	.1696	9.987
	1.020	.1482	323.5	.8624	189.8	.846	.749	.4190	.1070	.5902	.7361	.2024	13.331
	1.172	.1728	302.5	.9157	169.7	.850	.735	.4522	.1459	.5959	.7173	.2501	19.405
	1.271	.1897	286.0	.9371	161.4	.846	.723	.4632	.1530	.5920	.6980	.2818	23.808
	1.402	.2301	258.5	1.0948	127.8	.948	.747	.4386	.0904	.5540	.6913	.3544	35.280
	1.610	.2520	254.5	1.0412	126.3	1.077	.783	.3918	.0724	.5828	.6852	.3905	42.074
	1.505	.2359	225.5	1.0687	112.2	1.098	.733	.4399	.0633	.5256	.6340	.4047	41.339
14,000	.571	.0753	270.0	.6444	183.4	1.130	1.041	.1157	.0927	.8792	1.0368	.0827	2.966
	.726	.0975	254.0	.7087	165.2	.906	.918	.2830	.1844	.8036	.9151	.1111	4.626
	.814	.1127	238.0	.7563	144.0	.841	.773	.4281	.1574	.6315	.7647	.1442	6.322
	.927	.1305	222.8	.8416	129.2	.857	.768	.4544	.1509	.5987	.7565	.1722	8.805
	1.016	.1467	209.8	.8270	119.7	.866	.764	.4740	.1933	.6215	.7538	.1983	11.417
	1.098	.1602	220.2	.9977	110.8	.876	.732	.6453	.3178	.5747	.7343	.2259	14.296
	1.261	.1883	190.4	.9863	99.2	.931	.739	.4615	.1215	.5622	.6877	.2747	19.422
	1.221	.1831	180.8	1.0039	90.1	1.018	.730	.4815	.1039	.5246	.6647	.3969	21.937
24,000	.515	.0680	284.0	.5926	201.4	1.160	1.061	.2844	.2994	.9172	1.0598	.0779	2.787
	.664	.0900	262.3	.6645	176.1	1.011	.898	.4033	.2352	.7341	.8906	.1107	4.600
	.812	.1126	239.6	.7474	151.1	.903	.761	.4203	.1532	.6351	.7372	.1505	6.847
	1.040	.1480	221.1	.7879	129.5	1.168	.785	.3935	.0710	.5797	.6980	.2121	12.641
	.622	.0834	353.0	.6912	241.3	1.100	.956	.4886	.3062	.7998	.9621	.0923	3.830
	.788	.1086	308.5	.7942	197.2	.977	.844	.3866	.1716	.6872	.8306	.1308	6.332
	.858	.1176	291.0	.8454	181.5	1.010	.837	.4004	.1629	.6647	.8156	.1501	8.015
	.950	.1354	276.0	.8985	165.9	.986	.779	.4217	.1176	.5981	.7322	.1739	9.547
32,000	.558	.0741	238.0	.6290	163.3	.932	.838	.3784	.1802	.7040	.8302	.0842	2.374
	.616	.0824	242.9	.6534	162.6	1.098	.957	.2402	.1825	.8445	.9445	.0960	3.520
	.699	.0944	234.1	.6929	151.4	1.080	.945	.2565	.1551	.8008	.9161	.1126	4.632
	.725	.0992	232.5	.7097	146.0	1.213	1.026	.1614	.1250	.8658	.9910	.1211	5.789
	.810	.1122	227.1	.7583	140.1	1.182	.961	.2224	.0747	.7545	.8890	.1392	6.825
	.830	.1151	226.0	.7788	138.4	1.240	1.049	.1354	.0859	.8527	.9600	.1429	7.752

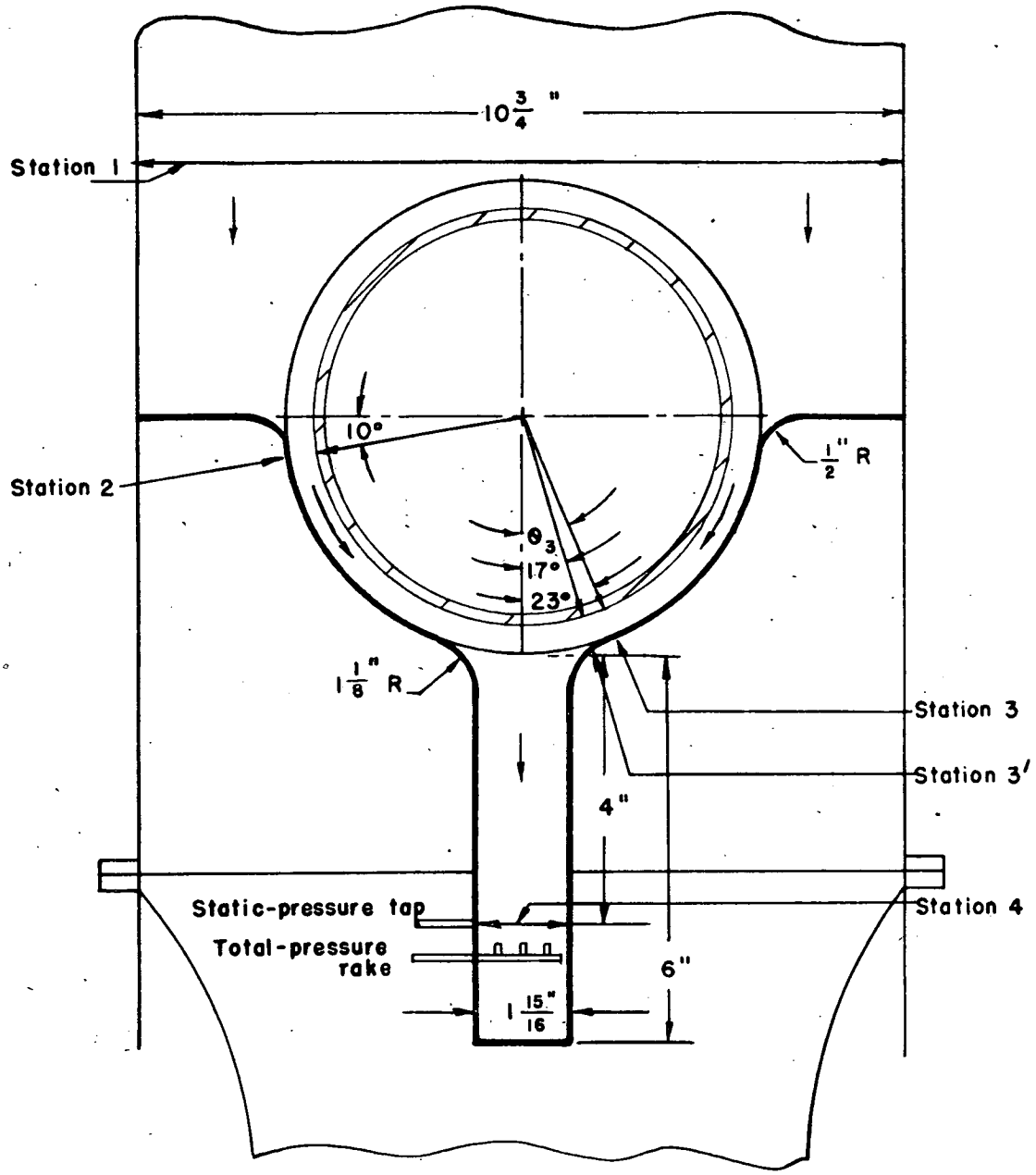

NATIONAL ADVISORY
COMMITTEE FOR AERONAUTICS

Figure 1.— Finned cylinder, baffles, tailpiece, and measuring-station locations used in tests.

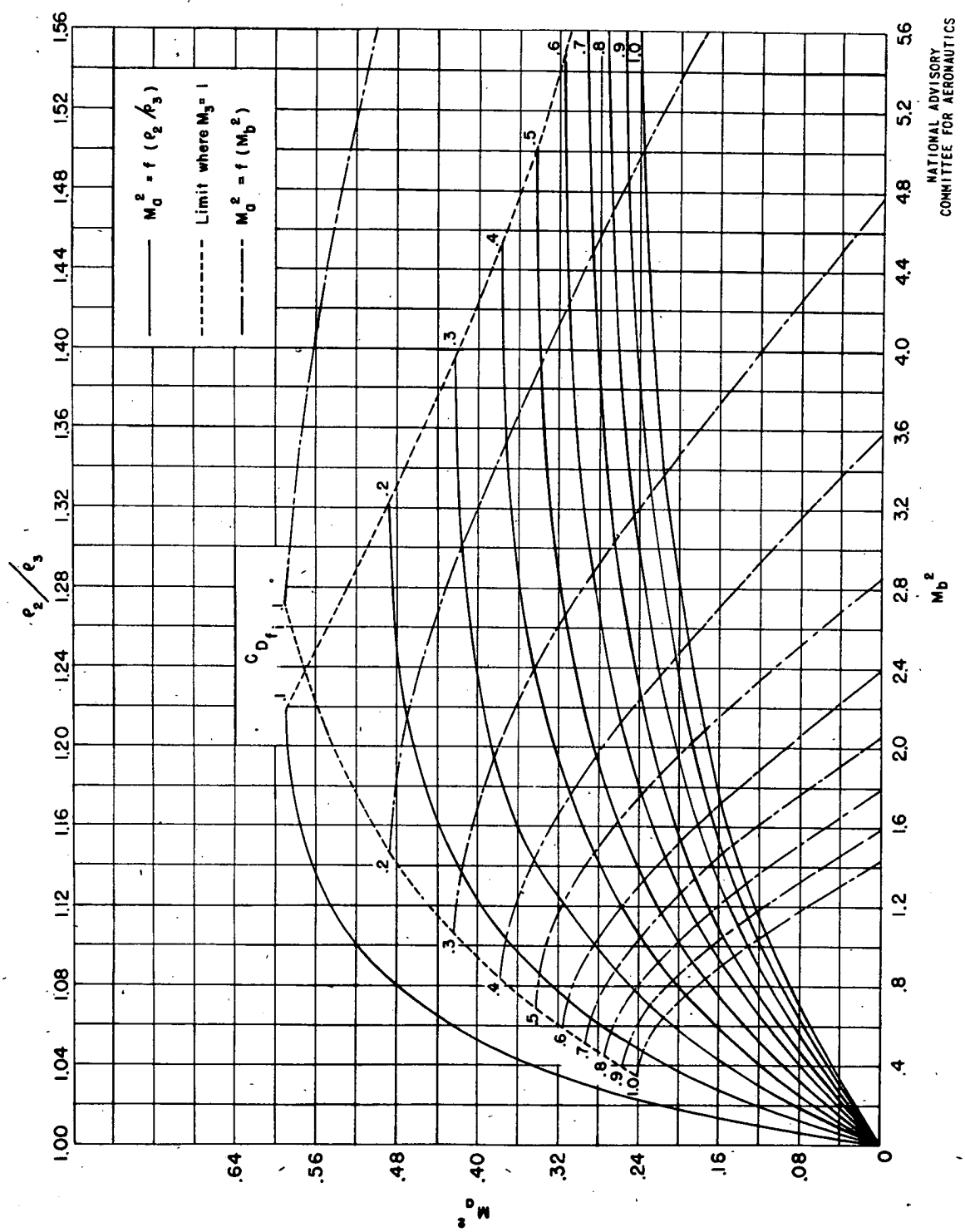

Figure 3.— Determination of ratio of density at station 2 to density at station 3. Parameters refer to values of $C_{D_{f_i}}$

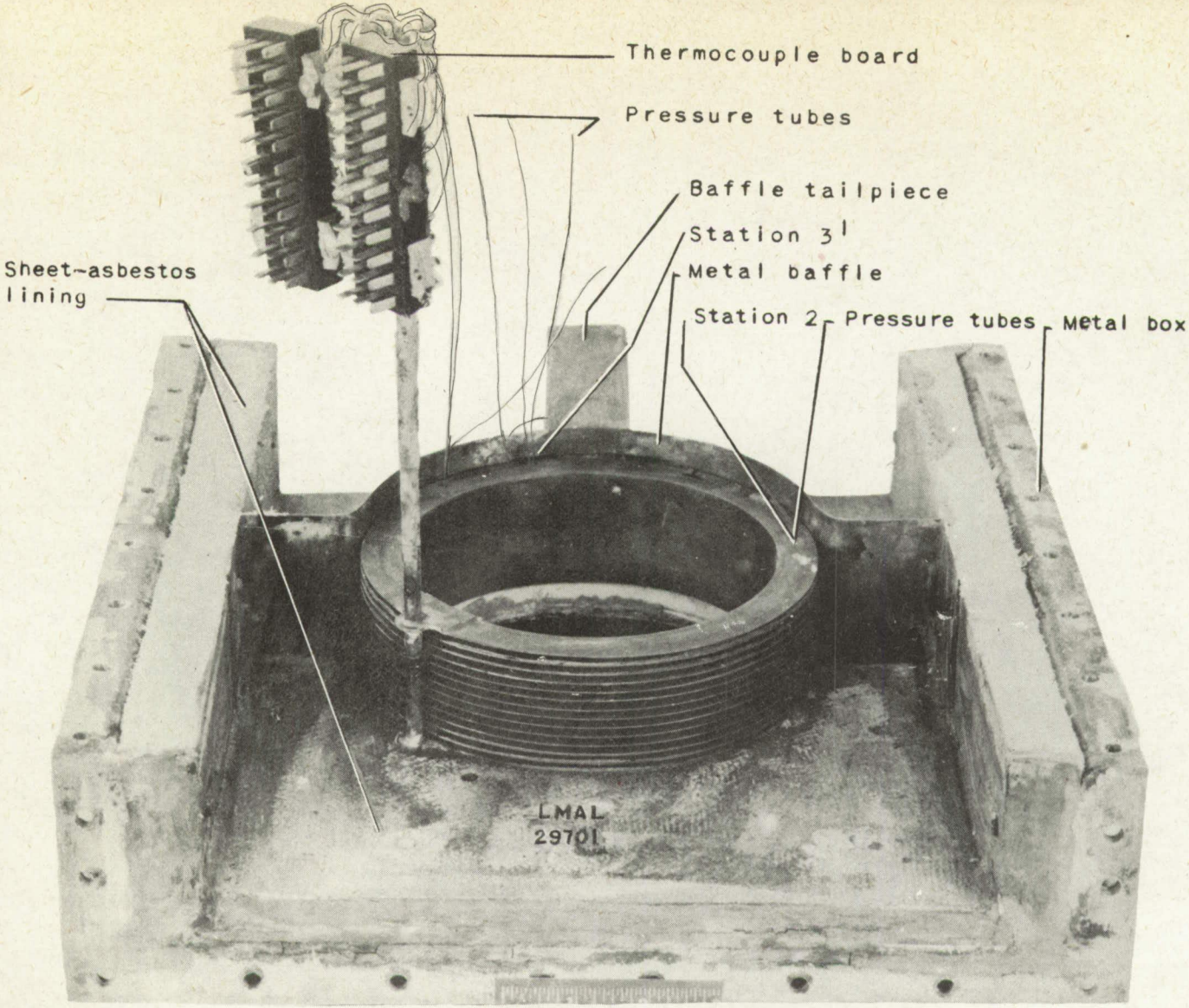

Figure 4. - Test unit showing test cylinder, baffles, tailpiece, insulated metal box, pressure tables, and thermocouples.

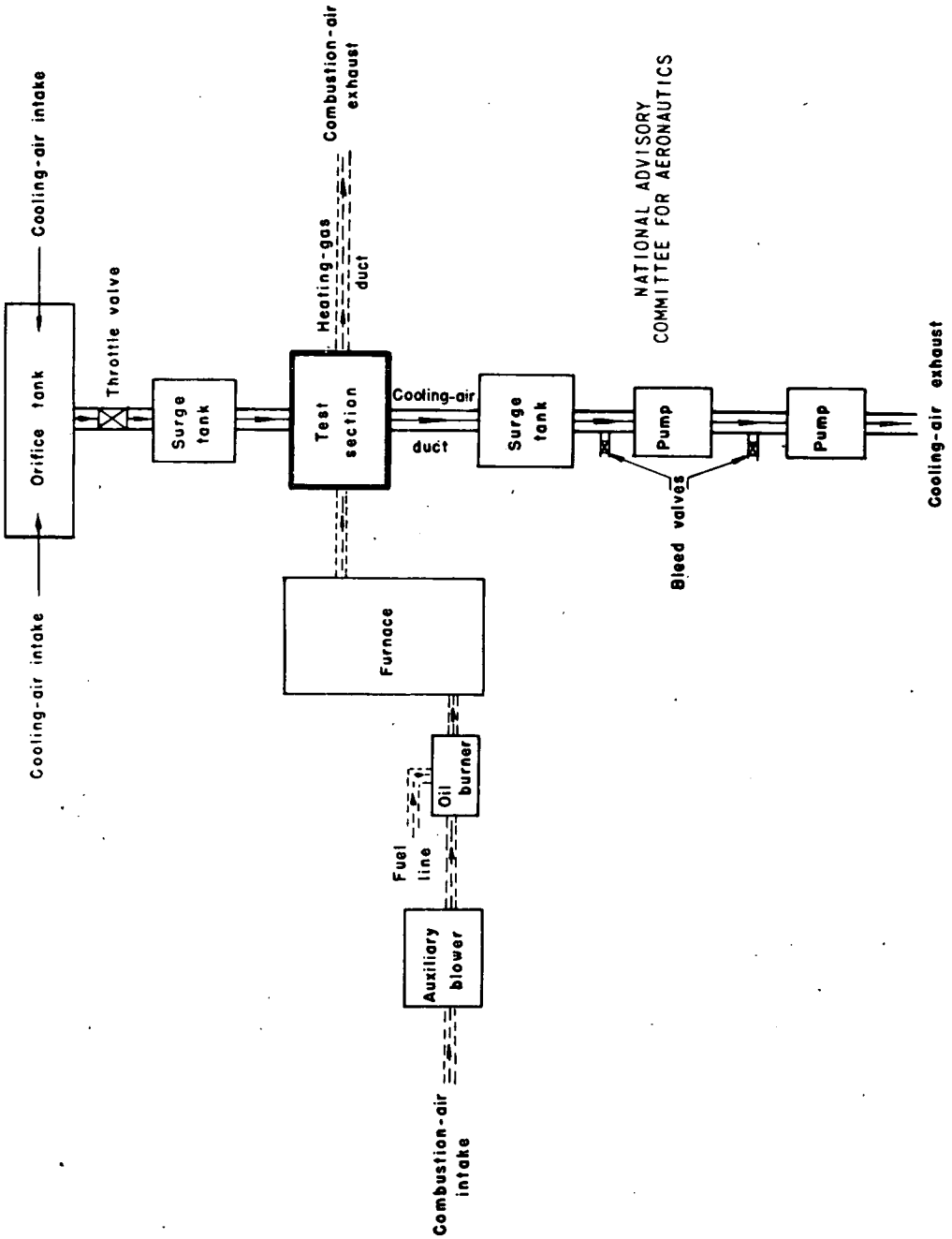

Figure 5.- Diagram of test setup.

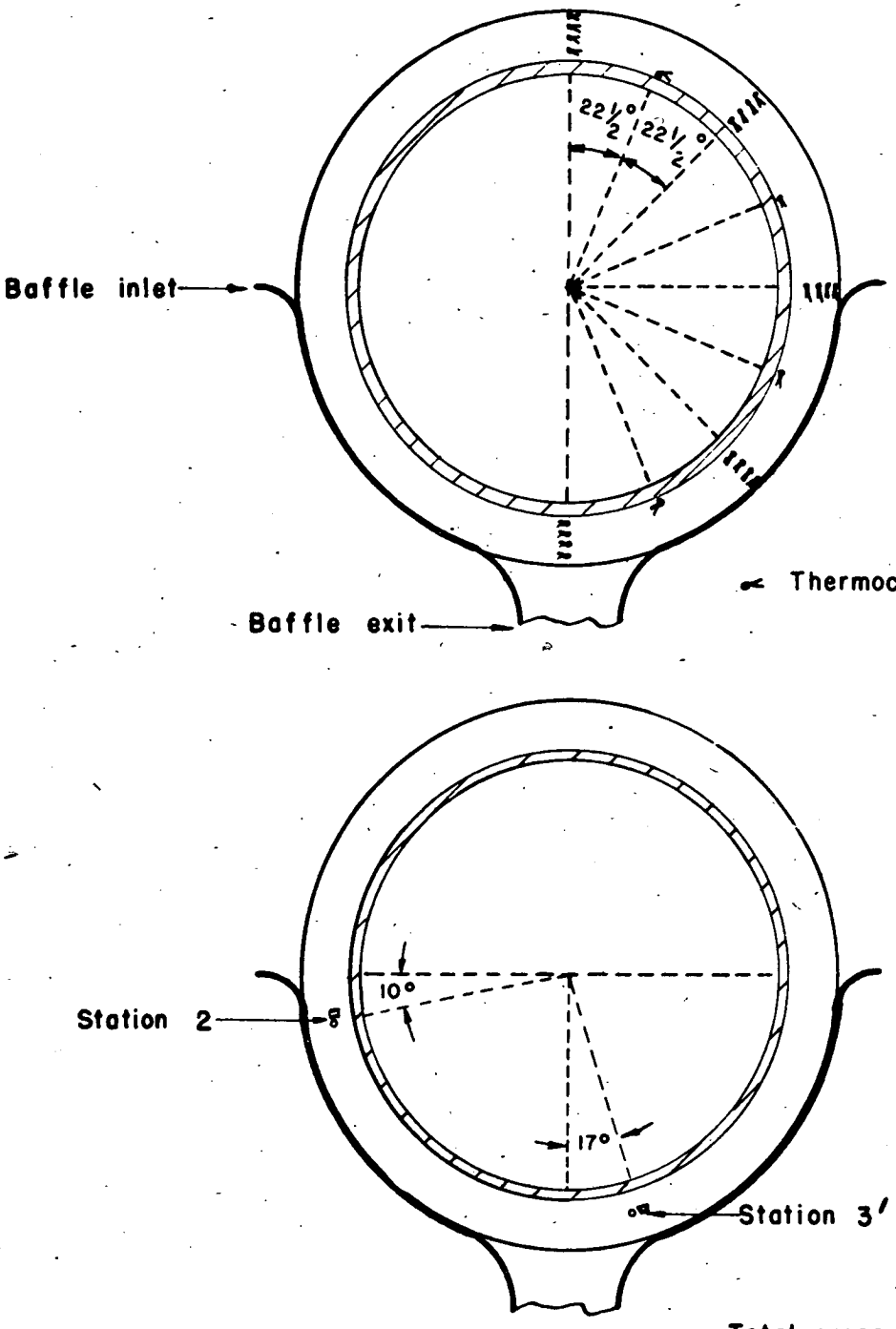

NATIONAL ADVISORY
COMMITTEE FOR AERONAUTICS

Figure 6.- Location of thermocouples and pressure tubes on test cylinder.

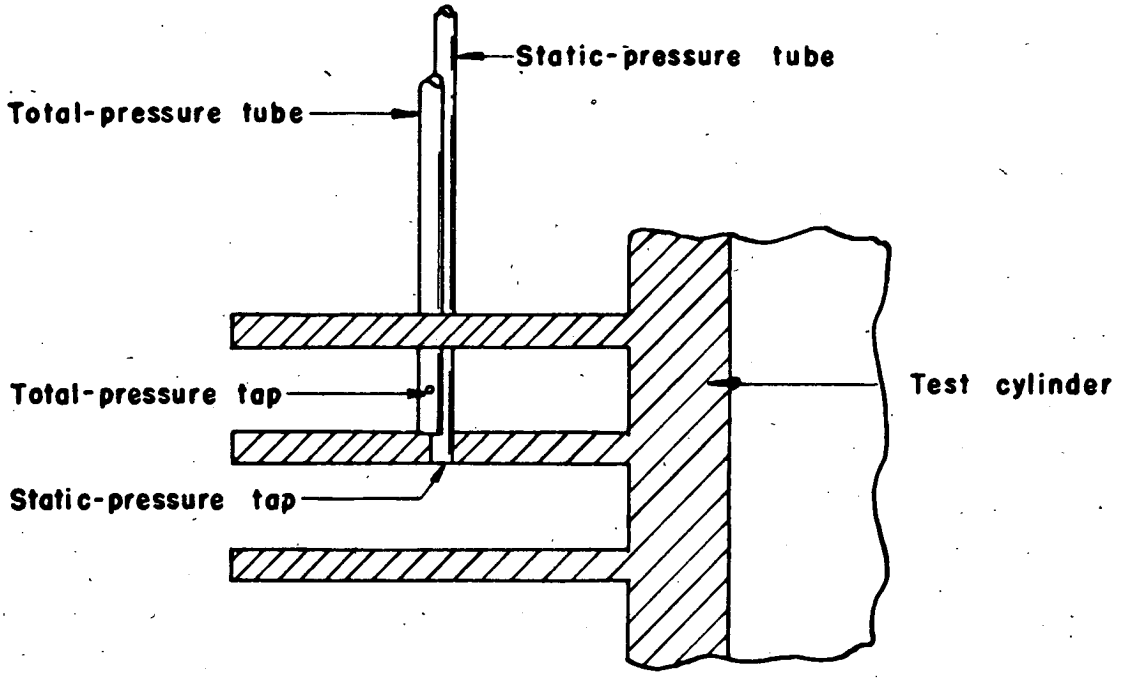

NATIONAL ADVISORY
COMMITTEE FOR AERONATUICS

Figure 7.— Sketch showing method of installing pressure tubes between fins.

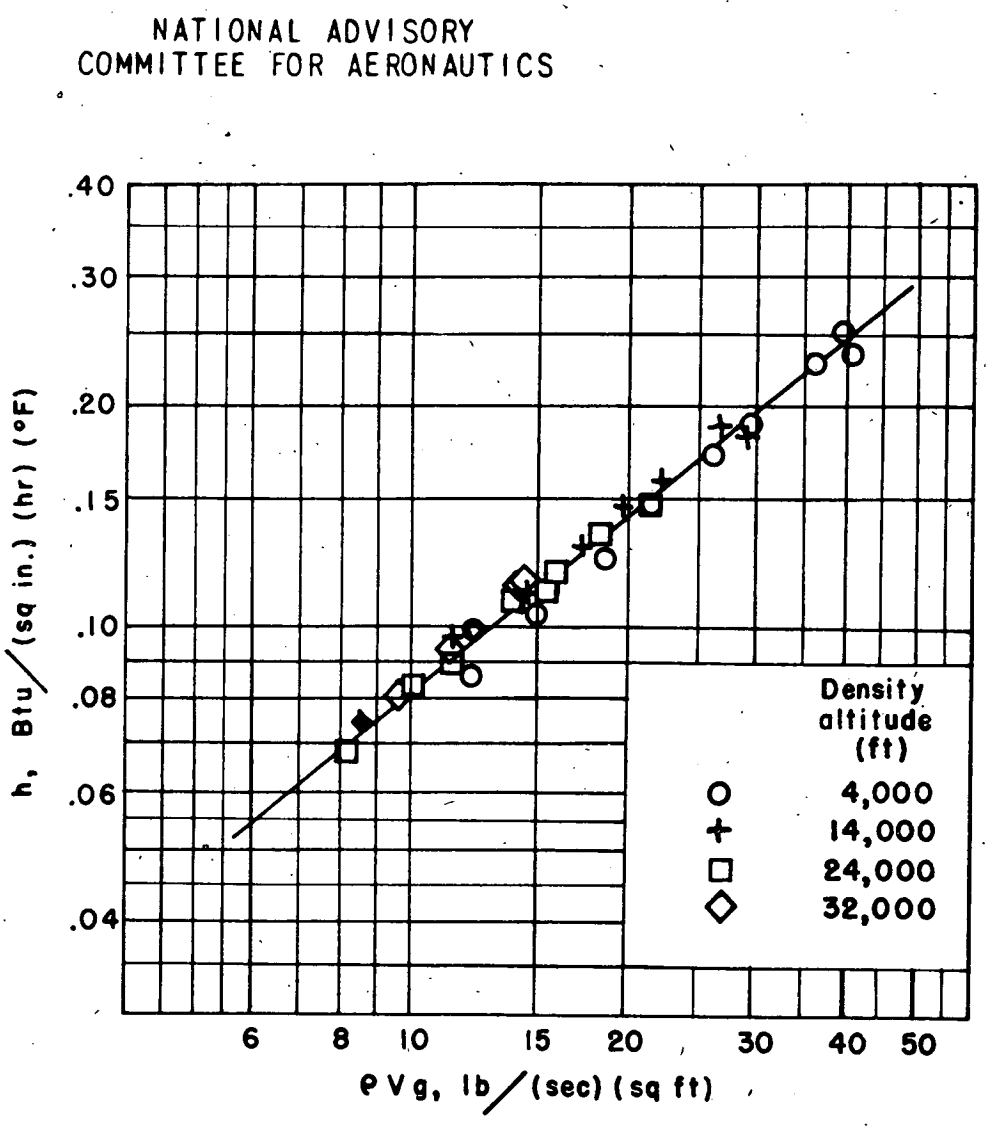

Figure 8.- Variation of surface heat-transfer coefficient with cooling-air weight flow.

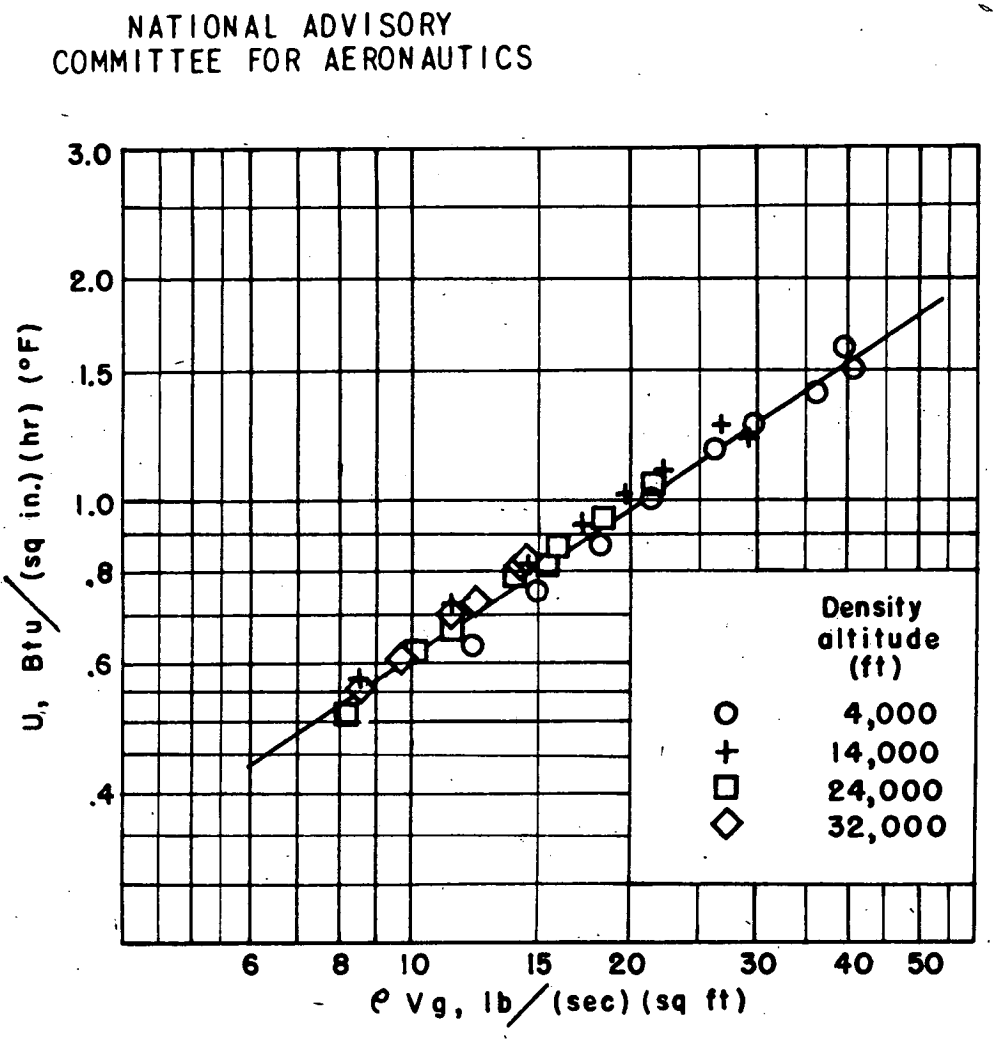

Figure 9.— Variation of over-all heat-transfer coefficient with cooling-air weight flow.

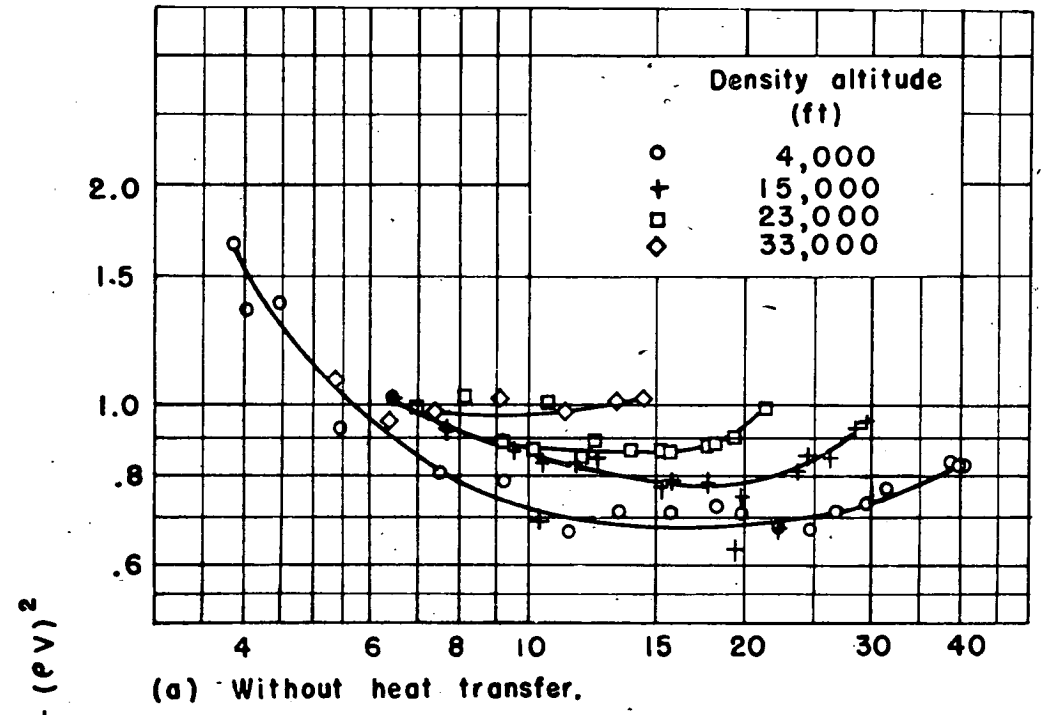

(a) Without heat transfer.

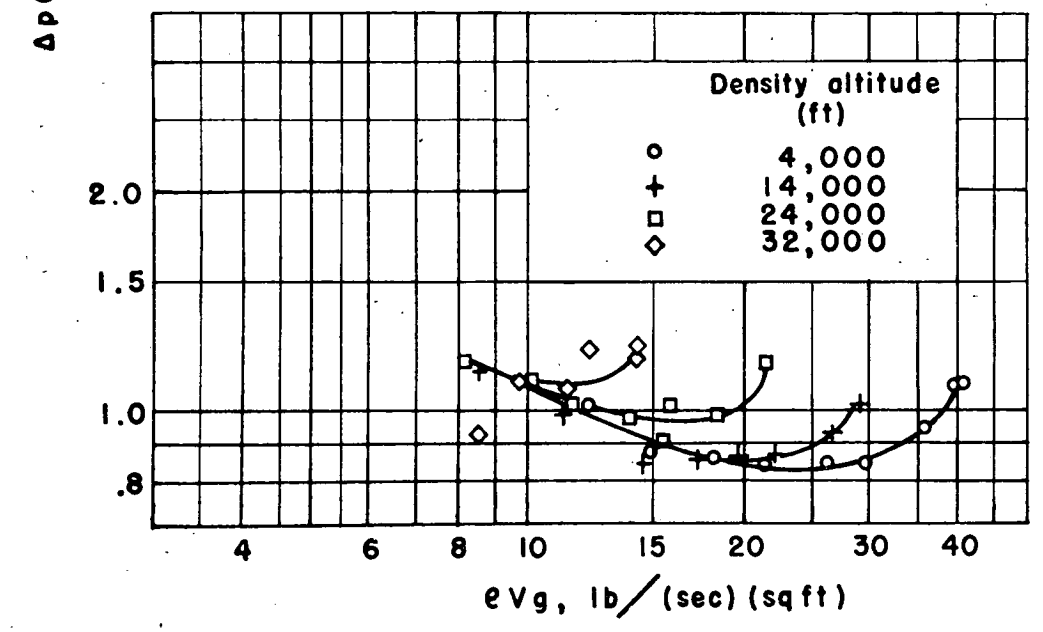

$\Delta p \rho_{av} / \frac{1}{2} (\rho V)^2$

(b) With heat transfer.

Figure 10.- Variation of pressure-loss function with cooling-air weight flow.

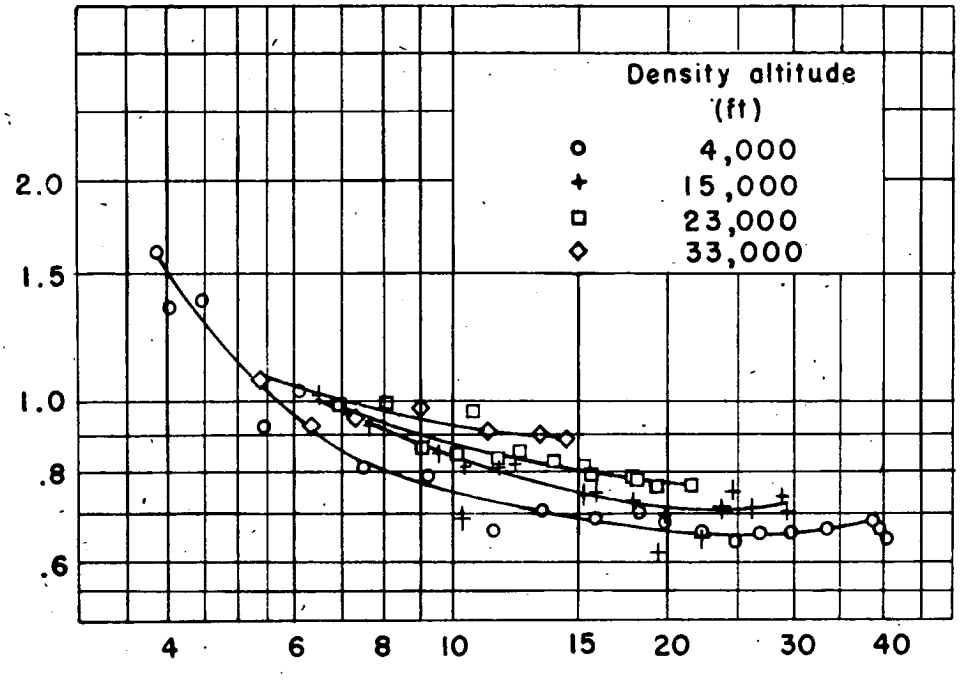

(a) Without heat transfer.

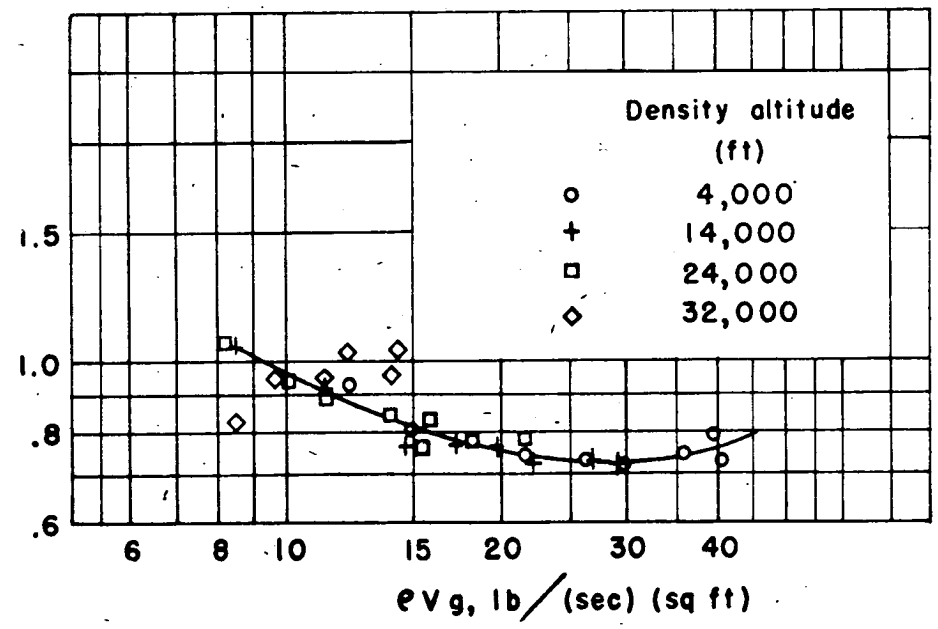

(b) With heat transfer.

Figure 11.— Variation of pressure-loss function with cooling-air weight flow.

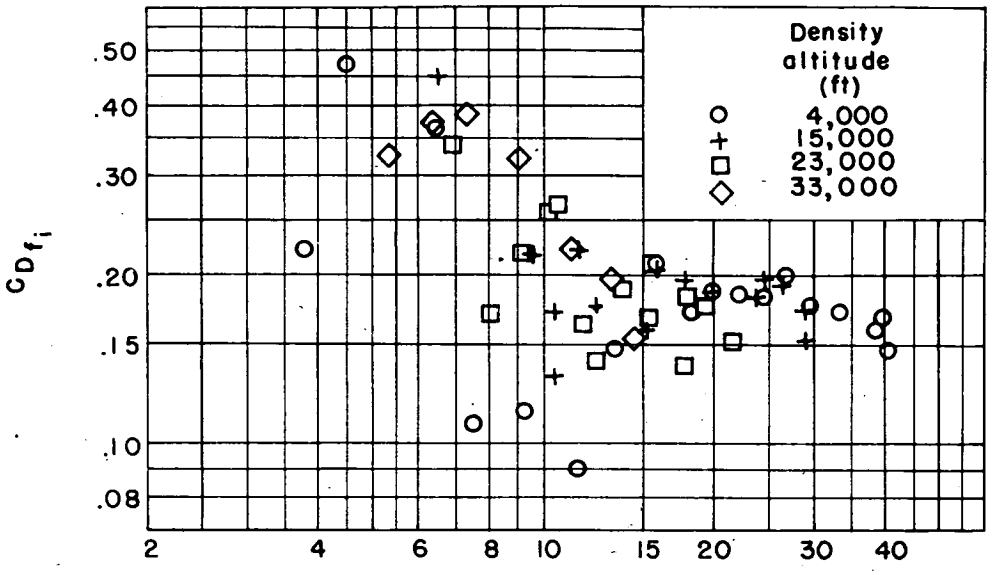

(a) Without heat transfer.

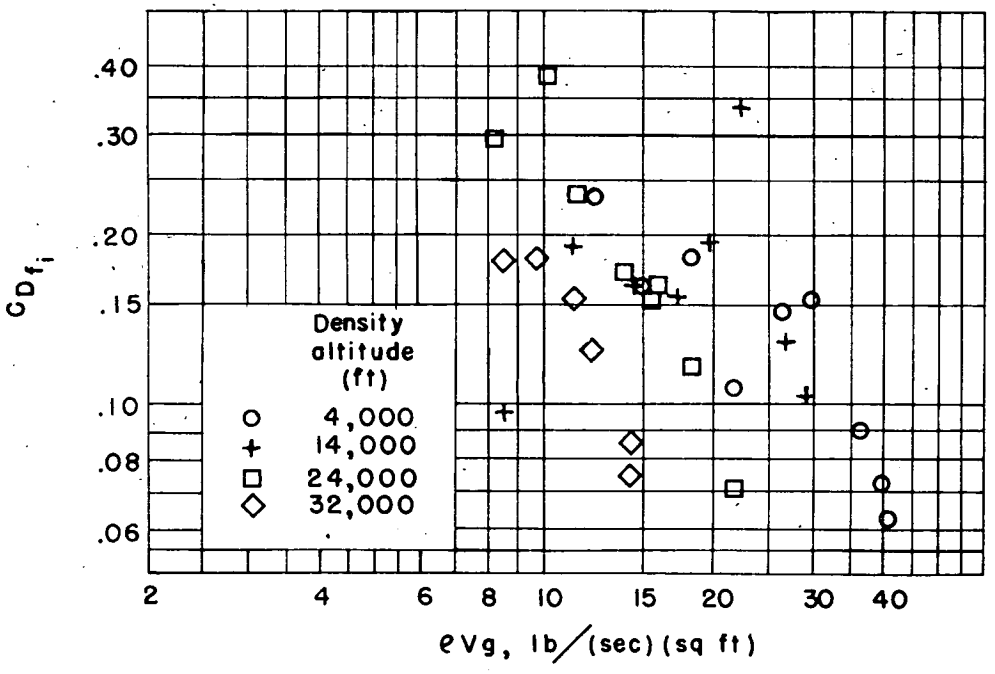

(b) With heat transfer.

Figure 12.— Variation of baffle-channel drag coefficient with cooling-air weight flow. Drag coefficient calculated from test data.

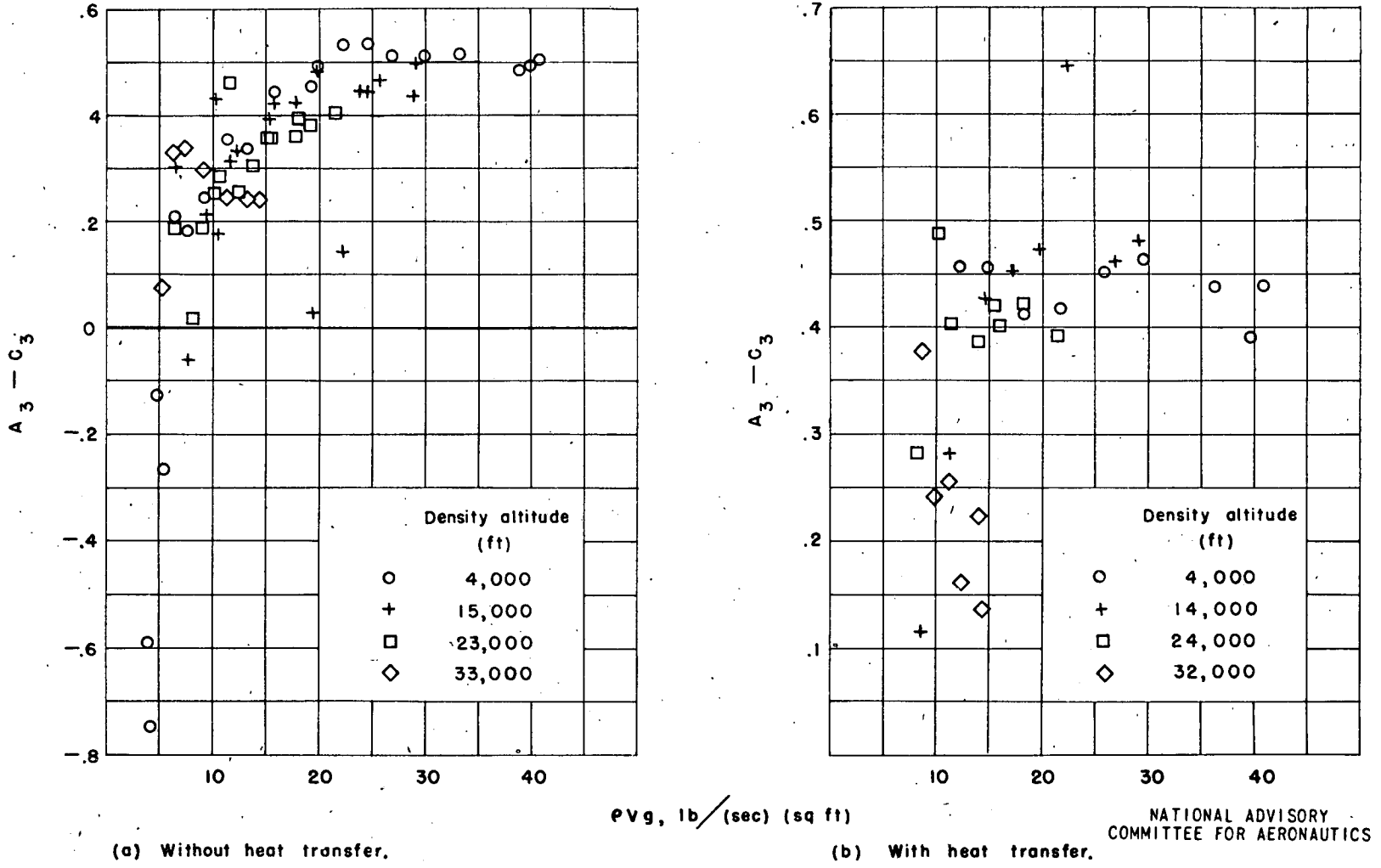

Figure 13.— Variation of exit coefficient with cooling-air weight flow.

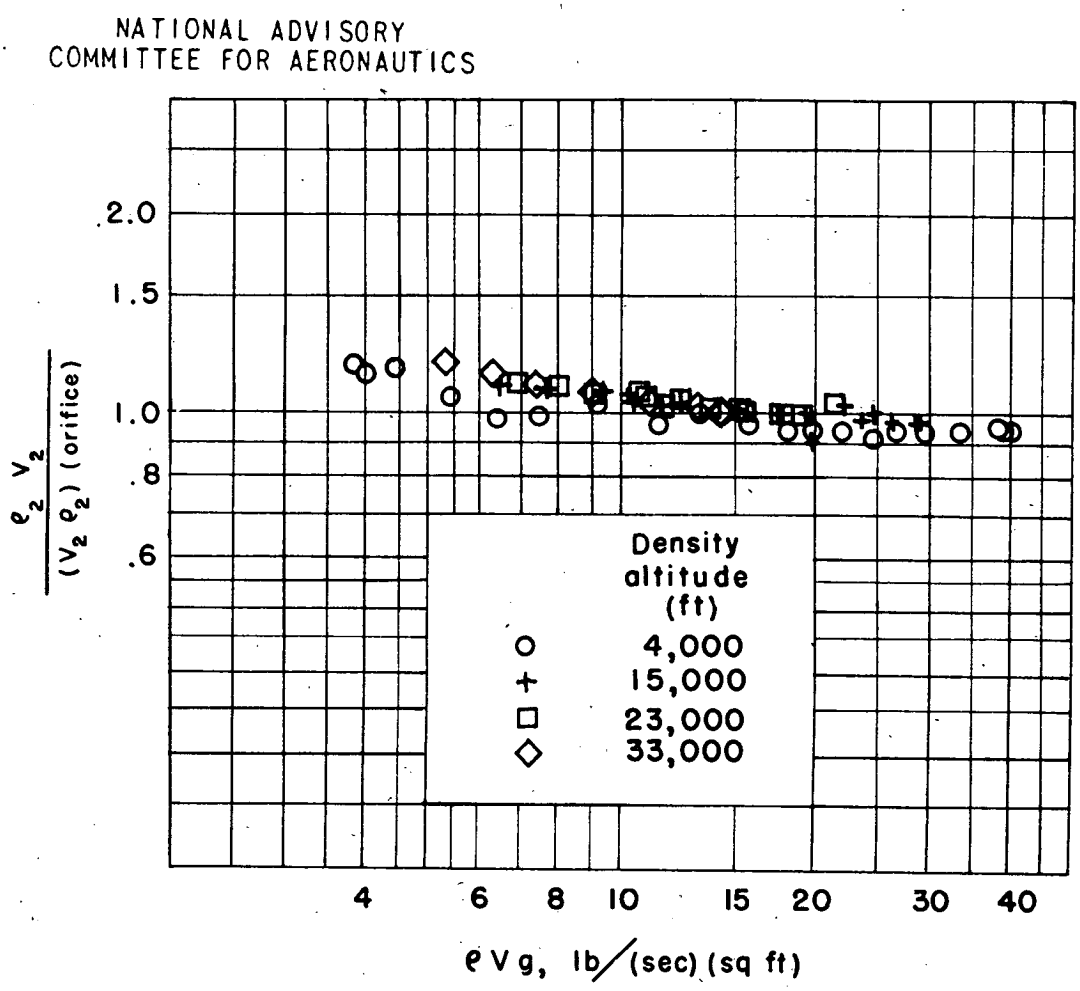

Figure 14.— Ratio of mass flow measured at station 2 to mass flow at station 2 obtained from orifice measurements. Tests made without heat transfer.

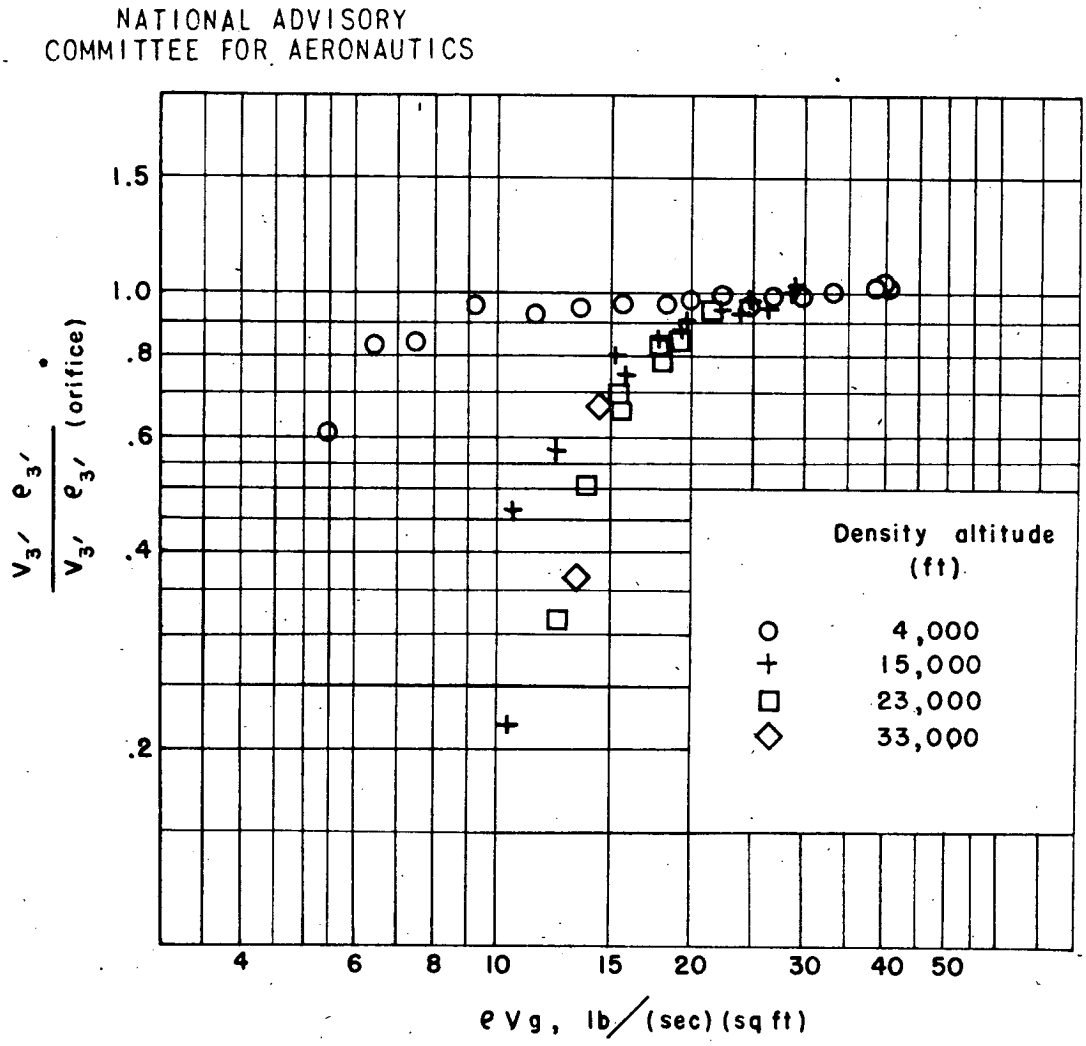

Figure 15.— Ratio of mass flow measured at station 3′ to mass flow at station 3′ obtained from orifice measurements. Tests made without heat transfer.

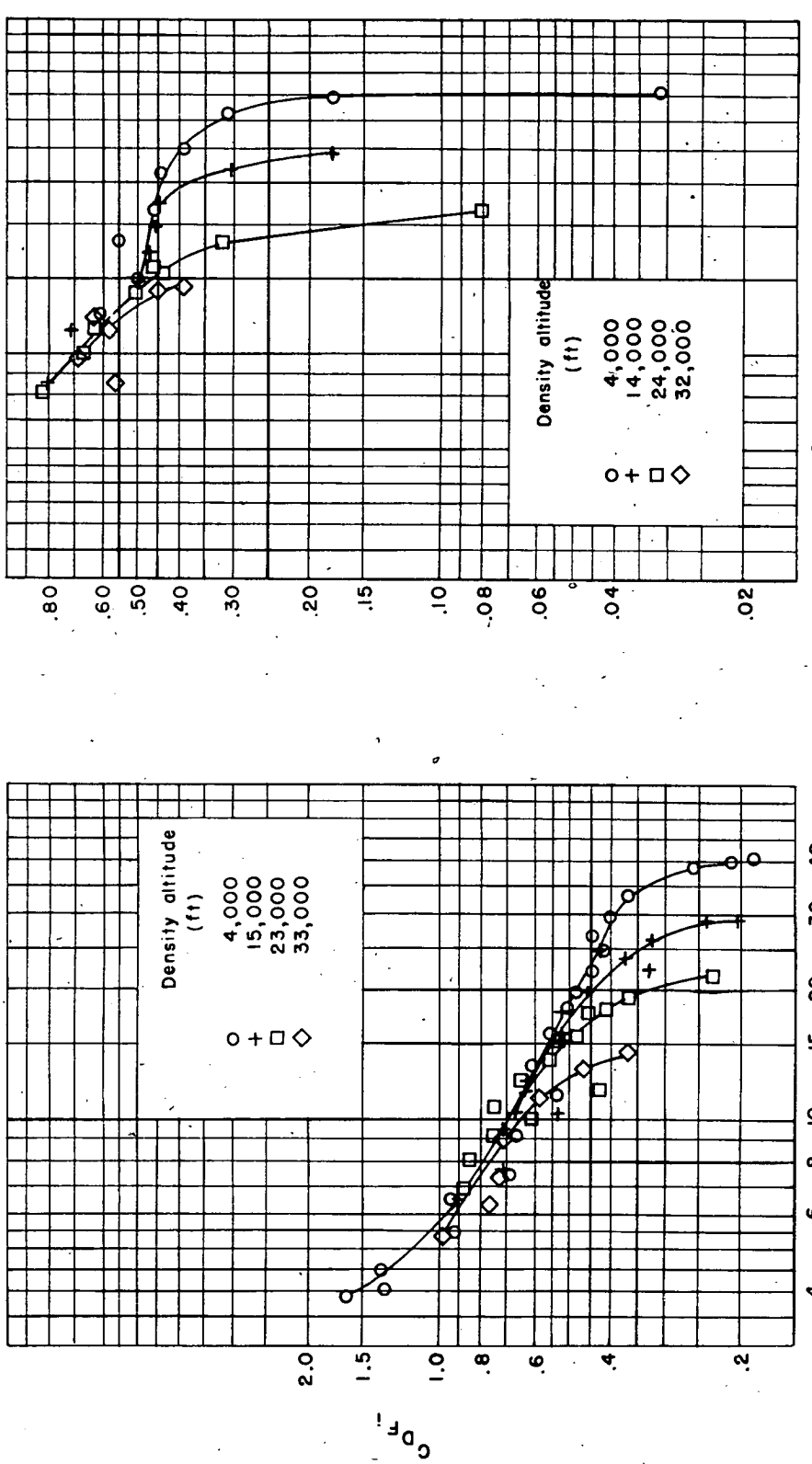

(a) Without heat transfer. (b) With heat transfer.

Figure 16.— Effect of cooling-air weight flow on friction-drag coefficient calculated by use of assumed exit loss.

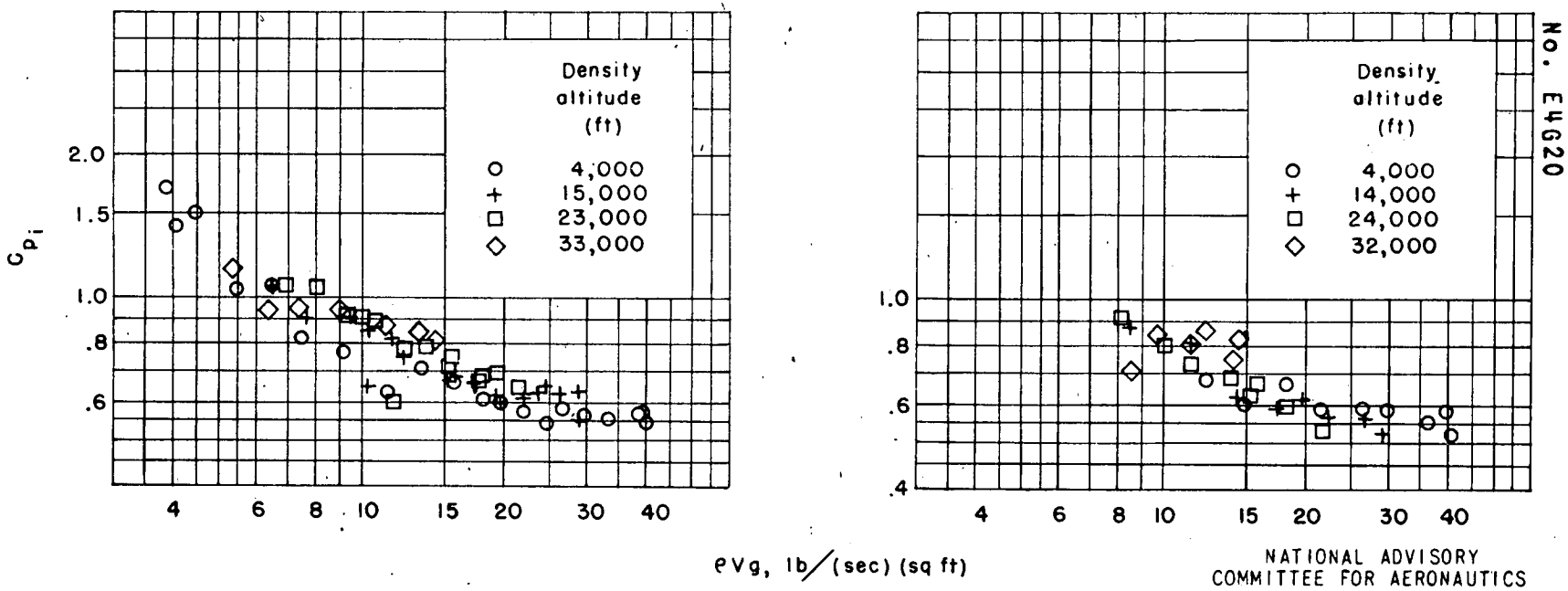

(a) Without heat transfer.

(b) With heat transfer.

Figure 17.— Effect of cooling-air weight flow on pressure-loss coefficient calculated from test data by analytical method.

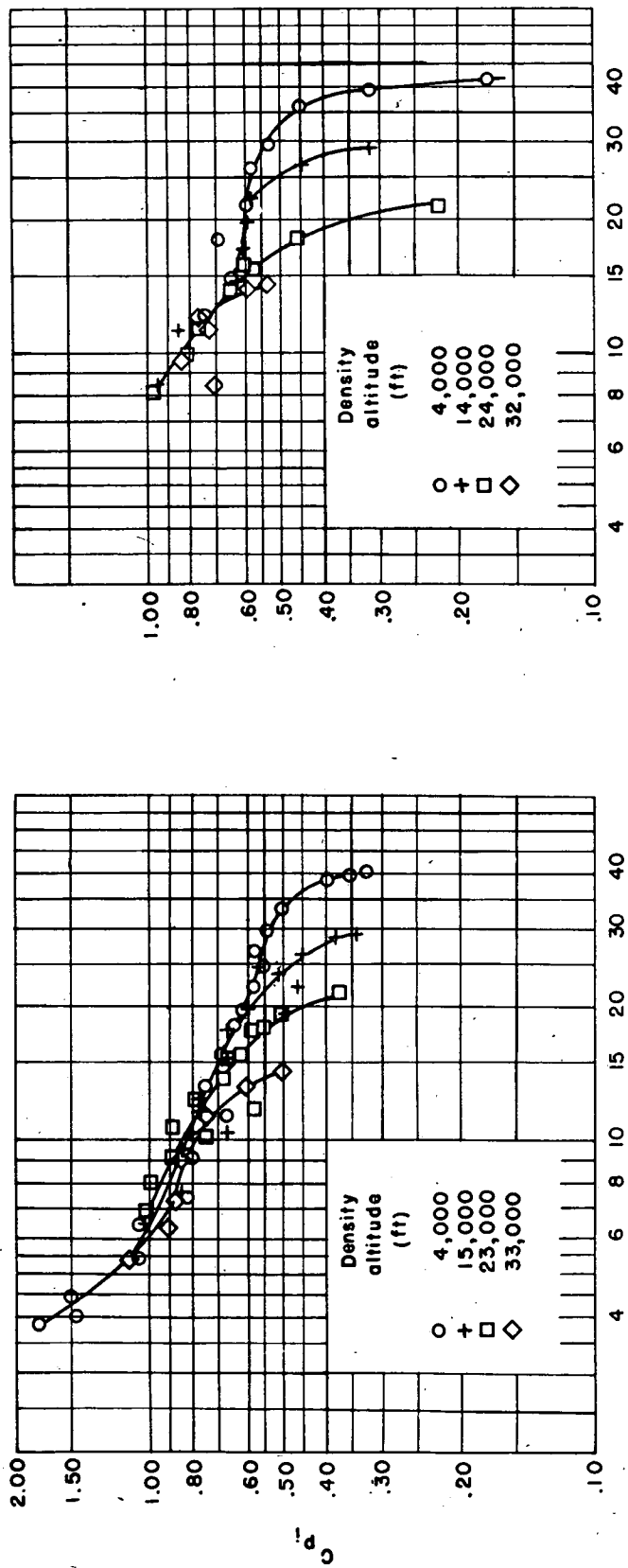

Figure 18.— Effect of cooling-air weight flow on pressure-loss coefficient calculated by use of assumed exit loss.

NATIONAL ADVISORY
COMMITTEE FOR AERONATUICS

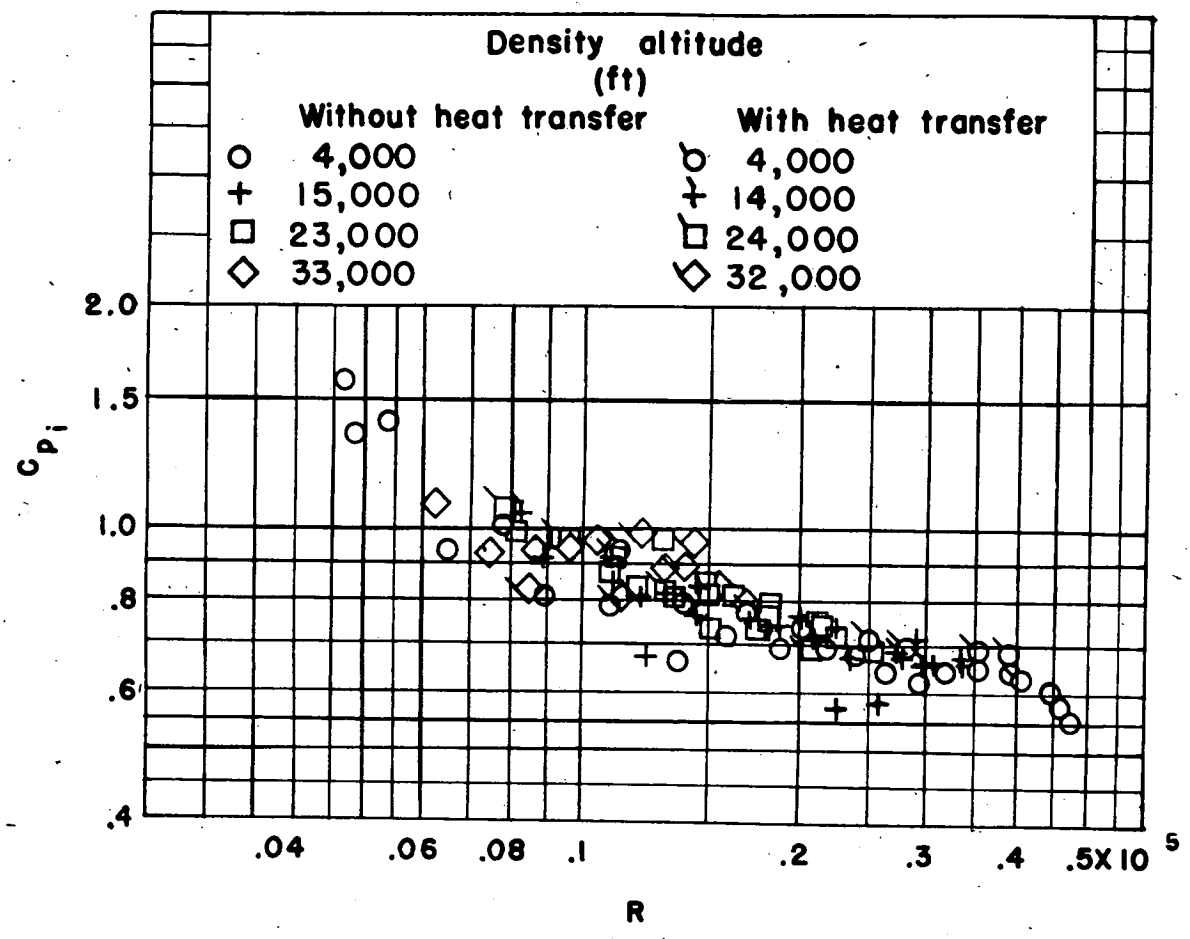

Figure 19.— Effect of Reynolds number on pressure-loss coefficient computed by empirical method.

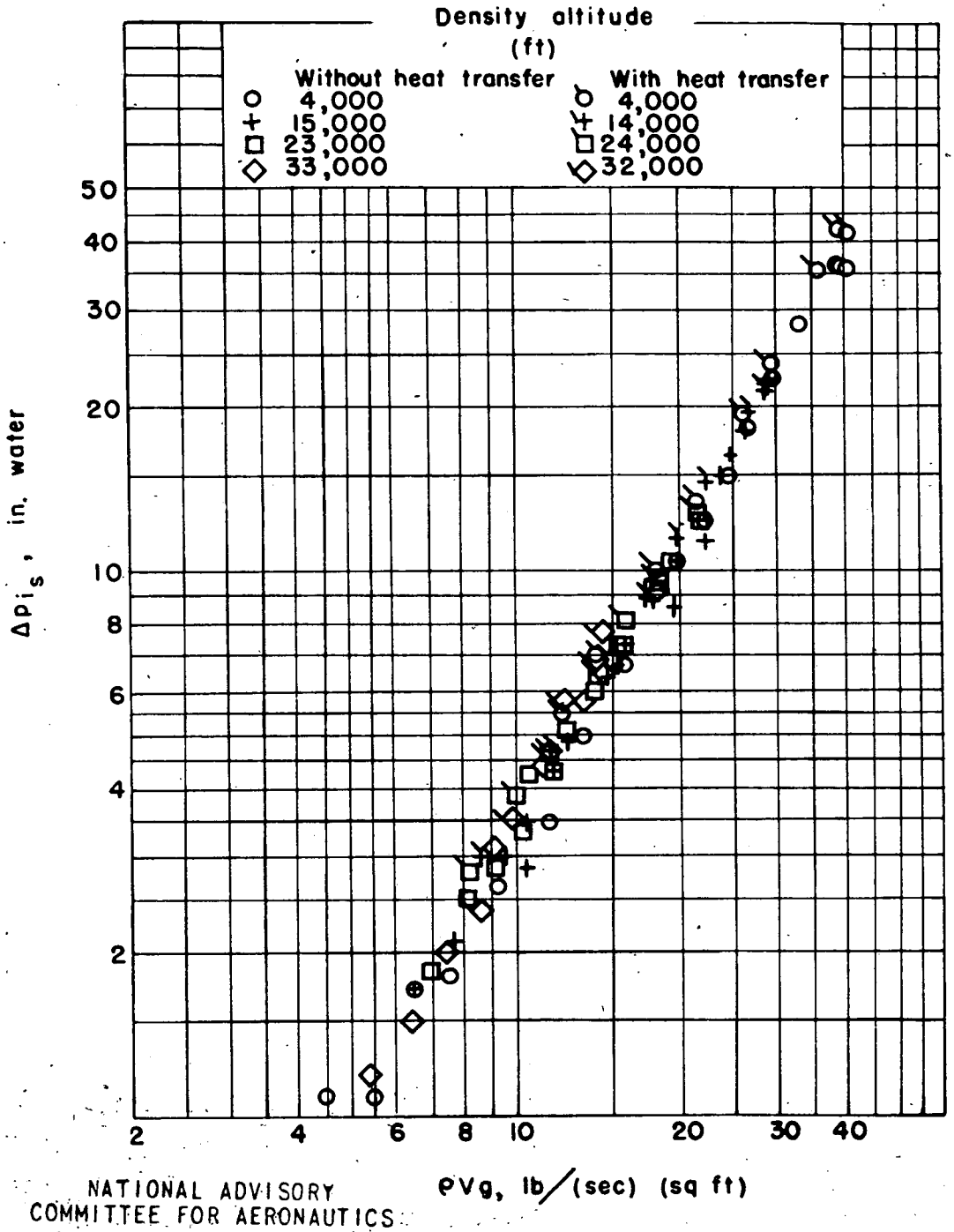

Figure 20.— Variation of corrected pressure loss with cooling-air weight flow.

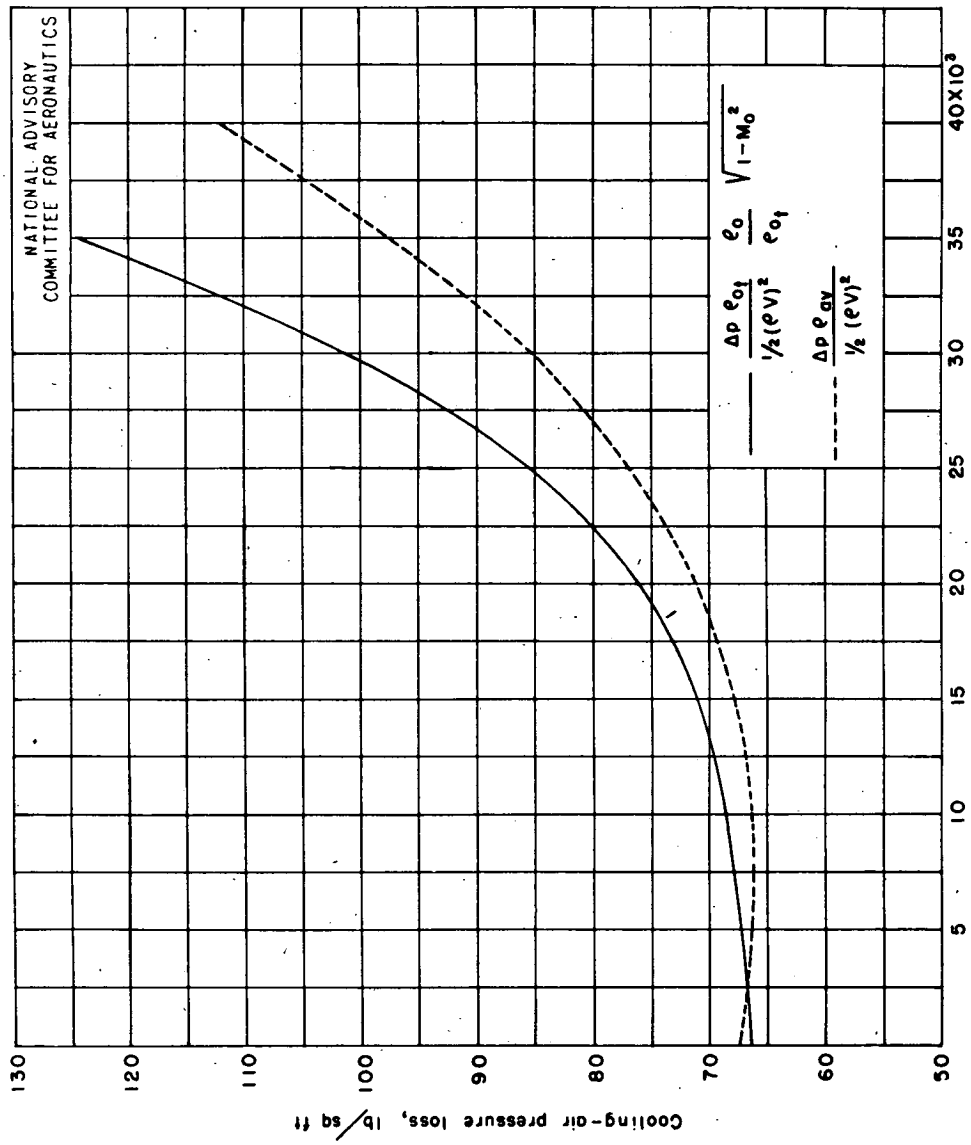

Figure 21.— Prediction of cooling-air pressure loss at altitude by use of $\frac{\Delta p\,\rho_{o_1}}{\frac{1}{2}(\rho V)^2}\,\frac{\rho_o}{\rho_{o_1}}\sqrt{1-M_o^2}$, assumed a function of Reynolds number, and by use of $\frac{\Delta p\,\rho_{av}}{\frac{1}{2}(\rho V)^2}$, assumed a function of mass flow.

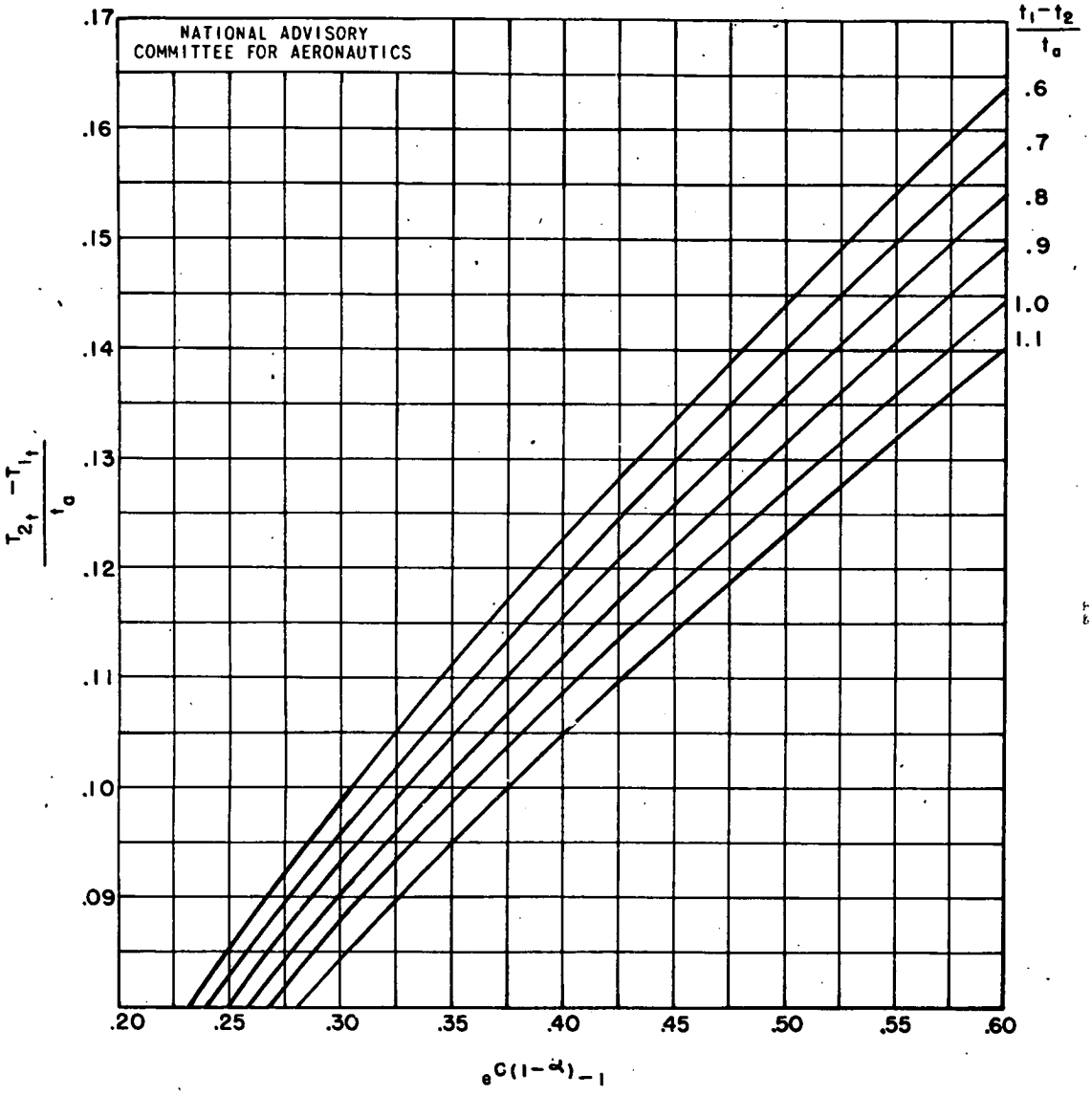

Figure 22.– Determination of $\frac{T_{2_t} - T_{1_t}}{t_a}$ $\alpha = \frac{5}{9}$